CHALMERS

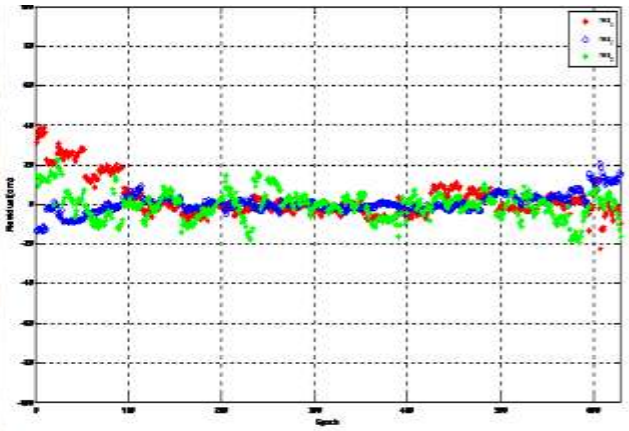

High Rate Kinematic GNSS Observations for Local-Tie Survey

Master of Science Thesis in the Master Degree Programme, Radio and Space Science

SYED REZWAN KABIR

Department of Earth and Space Sciences
Group of Space Geodesy and Geodynamics
CHALMERS UNIVERSITY OF TECHNOLOGY
Gothenburg, Sweden, 2011

Thesis for the Degree of Master of Science

High Rate Kinematic GNSS Observations for Local-Tie Survey

Syed Rezwan Kabir

Department of Earth and Space Sciences
CHALMERS UNIVERSITY OF TECHNOLOGY
Gothenburg, Sweden, 2011

‘High Rate Kinematic GNSS Observations for Local-Tie Survey’

Syed Rezwan Kabir

Supervisor

Dr. Rüdiger Haas
Associate Professor
Group of Space Geodesy & Geodynamics
Dept. of Earth and Space Science
Chalmers University of Technology
Onsala Space Observatory
+46 31 772 55 30
rudiger.haas@chalmers.se

Group of Space Geodesy and Geodynamics
Department of Earth and Space Sciences
Chalmers University of Technology
SE-412 96 Göteborg, Sweden

Cover: The figure on left shows the mounted GNSS antenna on top of the 20 meter radio telescope which is enclosed by a protecting radome. The figure on right shows the residual plot of the observations as a function of epoch.

Abstract

Onsala Space Observatory (OSO) is a fundamental geodetic station with co-located geodetic equipment. OSO takes part in the International VLBI Service (IVS) and the International GNSS Service (IGS) by a radome enclosed 20 meter radio telescope and a GNSS-monument and corresponding receiver, respectively. Additionally, a GNSS antenna was mounted on top of the 20 meter radio telescope in late 90's to determine the Invariant Point (IVP) of the telescope. The International Terrestrial Reference Frame (ITRF) is maintained by using measurements of several space geodetic techniques, VLBI, GNSS, Satellite Laser Ranging (SLR) and Doppler Orbitography and Radiopositioning Integrated by Satellite (DORIS). The global network of geodetic fundamental stations forms the backbone of the ITRF. To maintain the ITRF it is therefore very important to know the relative position of the geodetic equipments at these stations very precisely.

In order to measure the local-tie between the 20 meter radio telescope and the GNSS station at OSO several local-tie survey campaigns were performed since the 90's. But, except the most recent one performed in 2008, these survey campaigns did not provide the complete covariance information of the local-tie. In the 2002 and 2008 local-tie surveys, a hybrid technique was followed to determine the IVP of the 20 meter radio telescope. The problem with this approach is that it is very time consuming and needs various advanced equipment (i.e. Laser tracker, reflector, markers, ground pillars).

This master's thesis project was therefore to implement a more convenient technique to determine the IVP of the radio telescope at OSO. The indirect approach proposed by Finnish researchers to obtain the reference point of an azimuth-elevation type telescope was modeled and simulated in order to determine the IVP of the radio telescope. High-rate GNSS data observed with the antenna on top of the radio telescope were analyzed with a scientific GNSS processing software package. Both, GNSS-observations acquired during dedicated observing sessions and during standard telescope operation were analyzed with a kinematic approach. The corresponding results for the position of the GNSS-antenna were used to derive the IVP of the radio telescope.

Keywords: GNSS, ITRF, local-tie, reference point, VLBI, kinematic

Acknowledgements

First of all my greatest gratitude to Dr. Rüdiger Haas for supervising me throughout my thesis, whose guidance and support has been most appreciated and without whom this work would not have been possible. I would like to express special thanks to Dr. Jan Johansson and entire Space Geodesy and Geodynamics group. I would also like to thank Mr. K.M. Arif Aziz for supporting me with JAVA. I have enjoyed my work thoroughly both at Onsala Space Observatory and at the department of Earth and Space Sciences at Chalmers University of Technology over the past year.

I am thankful to my family and friends for all their support and encouragement. Last but not the least I dedicate this work to Rebekah for always being my inspiration.

Syed Rezwan Kabir
Gothenburg, Sweden
May 2011

Contents

CHAPTER ONE- INTRODUCTION

1.1 Objective

The earth is not a perfect sphere but a body that constantly changing its shape of the surface. To observe the motion of the earth crust, a permanent reference frame is required. The Terrestrial Reference Frame (TRF) provides the coordinates of a point on the earth surface with respect to the earth center. Modern space geodetic techniques such as Global Navigation Satellite System (GNSS), Very Long Baseline Interferometry (VLBI), Satellite Laser Ranging (SLR), Doppler Orbitography and Radiopositioning Integrated by Satellite (DORIS) are used to obtain the coordinates. International Terrestrial Reference Frame (ITRF) is the combination of individual TRF solutions. The ITRF is constantly updated. Onsala Space Observatory (OSO) contributes to the ITRF by observations with VLBI and GNSS. The local geometric relation between the reference points of the VLBI and GNSS equipment, and its potential change over time, are of major importance for the maintenance ITRF. Thus, there is a need to monitor this so called local-tie.

Since the radio telescope used at OSO for geodetic VLBI is enclosed by a protecting radome, any conventional local-tie survey with classical geodetic methods is difficult. Thus, in the late 90's a GNSS antenna was installed on top of the radome enclosed radio telescope. The idea of this installation is to determine the position of this GNSS antenna in a kinematic mode when the telescope is pointing to different directions, and use the different positions to indirectly derive the reference point of the radio telescope. One obvious disadvantage with this installation is that the current GNSS antenna tilts with the radio telescope and thus is not horizontal all the time during operations. Thus, the positions of the antenna phase center changes, and the satellite visibility is restricted.

The objective of the thesis is to develop a strategy to overcome antenna phase center variations caused by tilted GNSS antenna, implement a method to determine the reference point of the radio telescope indirectly and develop a MATLAB based analyzing software accordingly and compare the results with the past local-tie campaigns.

1.2 Local-Tie Survey

Geodetic fundamental stations are essential for the maintenance of the ITRF. The ITRF is realized by geodetic space techniques which are linked by local-ties at the observation stations *(Lösler and Eschelbach, 2009).* Geodetic solutions from the space geodetic techniques provide the geodetic and broader scientific community with complementary realizations of the TRF. The combination of these solutions provides the most accurate and stable global TRF suitable for geodetic applications *(Altamimi et al., 2002).* Hence it requires a reliable connection between the reference points of each system in a local reference frame. This connection is called local-tie. A meaningful combination and integration can only be achieved if the local-ties at these fundamental stations are known accurately *(Löser and Haas, 2009).* The requirements for the

reference points are that they are known with an accuracy of better than 1 mm *(Niell et al., 2006).* However, for most of the geodetic sites the reference points of the geodetic techniques are not measured precisely (i.e. sub mm level) and complete local tie information is also unavailable (i.e. covariance matrix of the coordinate observations).

The Invariant Point (IVP) or reference point of an azimuth and elevation type telescope is a fixed point to which position of the telescope is referred defined by the intersection point of the axes. An IVP can also be defined as the intersection of the primary axis (i.e. fixed axis) with the perpendicular vector between the secondary axis (i.e. moving axis) and primary axis *(Dawson et al., 2007).*

The measurement method for a local-tie vector depends on the site location and instruments. In practice there are three types of method adopted to determine the reference point of an azimuth elevation type telescope. These are as follows: direct method, hybrid method and indirect method. In the direct method the reference point is a geodetic marker that can be measured directly. In the hybrid or the classical method the reference point cannot be measured directly. Some surveying targets are fixed on the telescope to make the axis visible for pointing of the surveying instrument. The indirect method is entirely based on observed positions of targets fixed on solid structure of the telescope *(Kallio and Pountanen, 2010).* GNSS observations are done to measure the position of the targets when the telescope rotates around its axis.

1.3 Onsala Space Observatory

The Onsala Space Observatory (OSO) is a fundamental geodetic station that hosts co-located equipments for various geodetic techniques such as VLBI, GNSS. Currently the observatory is operating a 25 meter radio telescope, a radome enclosed 20 meter radio telescope and a permanent GNSS station. OSO has been contributing in space geodesy since late 60's. The very first geodetic VLBI experiment was performed at Onsala in the spring of 1968 *(Whitney, 1974).* The radome enclosed 20 meter radio telescope was constructed and during the transition period both telescopes were used for geodetic VLBI observations, observing in parallel but separately on X-band and S-band (*Haas and Eschelbach, 2005*). The 20 meter telescope is used for observation in both frequencies since 1987. A monument for a GPS antenna was constructed and acts today as reference monument for the Swedish ground-based GPS network SWEPOS and the IGS *(Haas and Eschelbach, 2005).* In the late 90's an additional GNSS antenna was mounted on top of the radome enclosed 20 meter radio telescope.

Figure 1.1: The IGS station (top-left), the radome enclosed 20 meter radio telescope (top-right), the 25 meter radio telescope (bottom-left), the GNSS antenna on top of the 20 meter radio telescope (bottom- right)

1.3.1 The 2002 Local-Tie Survey Campaign at OSO

The reference point of the radome enclosed 20 meter radio telescope at OSO cannot be measured directly. The IVP of the radio telescope exists somewhere inside the telescope receiver cabin. It thus can only be measured by indirect surveying methods *(Haas and Eschelbach, 2005*). In order to measure the local-tie vector at OSO several classical geodetic campaigns in 90'ies were performed. However these local-tie surveys did not provide complete covariance information. In 2002 a classical geodetic measurements were performed along with GPS measurements in the local network. A complete survey was carried out in two different epochs. For the epoch-1 several survey markers were installed inside the radome to determine the endpoints of the elevation axis for different azimuth directions and for epoch-2 magnetic survey markers were installed on the telescope cabin that acts as synthetic elevation axis endpoints. Later the reference point of the radio telescope was determined by 3D circle fitting to the elevation axis end points. The ground markers and survey pillars were connected to the local network along with IGS reference point (reference point of the IGS station is a steel bolt installed in solid bedrock below the GNSS antenna which is installed permanently on a concrete pillar) *(Haas and Eschelbach, 2005).* The coordinates of the reference point in the local reference frame were derived with standard deviations on the order of 0.1 mm in all three components for epoch-1 and 0.1 mm for

the horizontal components and 0.3 mm for the vertical component in epoch-2 *(Haas and Eschelbach, 2005).*

Station	X (m)	σ_x(mm)	Y(m)	σ_y(mm)	Z(m)	σ_z(mm)
IGS	12.7535	±0.2	23.3877	±0.1	9.0455	±0.6
IVS	90.1237	±0.1	35.9493	±0.1	22.7594	±0.1

Table 1.1: IGS and IVS reference points and their standard deviations in the local reference frame (Haas and Eschelbach, 2005)

1.3.2 The 2008 Local-Tie Survey Campaign at OSO

The 2008 local-tie survey campaign was also a classical geodetic measurement. This time a laser tracker was used as survey instrument. The use of a laser tracker provides highly accurate local-tie results on the sub-mm level *(Lösler and Haas, 2009).* A complete description of 2008 local-tie campaign can be found in *Lösler and Haas (2009)* and *Lösler and Eschelbach (2009).*

Station	X (m)	σ_x(mm)	Y(m)	σ_y(mm)	Z(m)	σ_z(mm)
IVS	90.12325	±0.10	35.94974	±0.10	22.75947	±0.08
IGS	12.75551	±0.21	23.39043	±0.25	9.06529	±0.27

Table 1.2: IVS and IGS reference points in local reference frame and their standard deviations (Lösler & Haas, 2009)

The distance between the reference points of the IVS station and the IGS station was also measured and compared with the 2002 campaign. This distance is independent of reference frame

As described earlier the IVP of an azimuth and elevation telescope is the intersection point between the axes. However, in practice the axes do not intersect. The offset vector can be described as the distance between the azimuth and elevation axis.

Distance between IVS and IGS reference points measured in 2002 and 2008 and axis offset of the radio telescope:

Campaign	Distance, d(m)	Axis offset, e (mm)
2002	79.5685	-6.0
2008	79.5678	-6.2

Table 1.3: Comparison of distance between reference points and axis offset of the radio telescope (Lösler & Haas, 2009)

CHAPTER TWO- GLOBAL NAVIGATION SATELLITE SYSTEMS

2.1 General Concept

In general Global Navigation Satellite Systems (GNSS) are the combination of different multi-satellite navigation systems. In other words, GNSS are the modern day positioning system developed and operated by different countries such as Global Positioning System (GPS) developed by United States, The Russian navigation system, Globalnaya Navigatsionnaya Sputnikovaya Sistema (GLONASS), Galileo, currently being built by European Union (EU) and European Space Agency (ESA) and the Chinese navigation systems, COMPASS/BeiDou. However, today only GPS is the only fully operational GNSS *(Löfgren, 2011).*

	GPS	**GLONASS**	**Galileo**	**COMPASS**
Affiliation	United States	Russia	Europe	China
Satellites	32(24)[a]	23(24)[a]	2(27)[a]	1(27)[a]
Orbital planes	6	3	3	3[b]
Orbital height (km)	20200	19100	23222	21150
Orbital period	11 h 28 min	11 h 15 min	14 h 7 min	~12 h 50 min
Orbital inclination	55°	64.8°	58°	55.5°
Multiple access	CDMA	FDMA[c]	CDMA	CDMA
Carrier frequencies (MHz)	1575.42 1227.60 1176.45	1598.06-1605.38 1242.94-1248.63	1575.42[d] 1278.75[d]	1561.098 1589.742 1207.140 1268.520
Current status	Fully operational	Partly operational	In preparation	Partly operational[e]

Table 2.1: Various GNSS, where only GPS is fully operational GNSS (Löfgren, 2011)

a: Number of satellites for a fully operational space segment.

b: Number of orbit planes for COMPASS/BeiDou Medium Earth Orbit constellation.

c: In the future, GLONASS will in addition to transmitting FDMA signals on the L1 and L2 bands also transmit CDMA signals on L1 and L2, *see Inside GNSS (2010).*

d: Galileo satellites are planned to broadcast 10 different navigation signals in the band 1.1-1.6 GHz, *see ESA Galileo Navigation (2007).*

e: COMPASS/BeiDou will have regional coverage with 5 Geostationary, 3 Inclined Geosynchronous and 4 Medium Earth Orbit satellites *(Chong, 2009).*

In this thesis work GPS was used extensively. Therefore a short description about the technology can be found in the next sections.

2.2 The Global Positioning System

The Global Positioning System (GPS) is a satellite based navigation system developed by United States Air Force. However, now it is used for both military and civil purpose. GPS provides continuous positioning and timing information anywhere in the world under any weather conditions *(El-Rabbany, 2002).* GPS is a passive system where users receive satellite signals only. GPS has three segments: space, control and user segment.

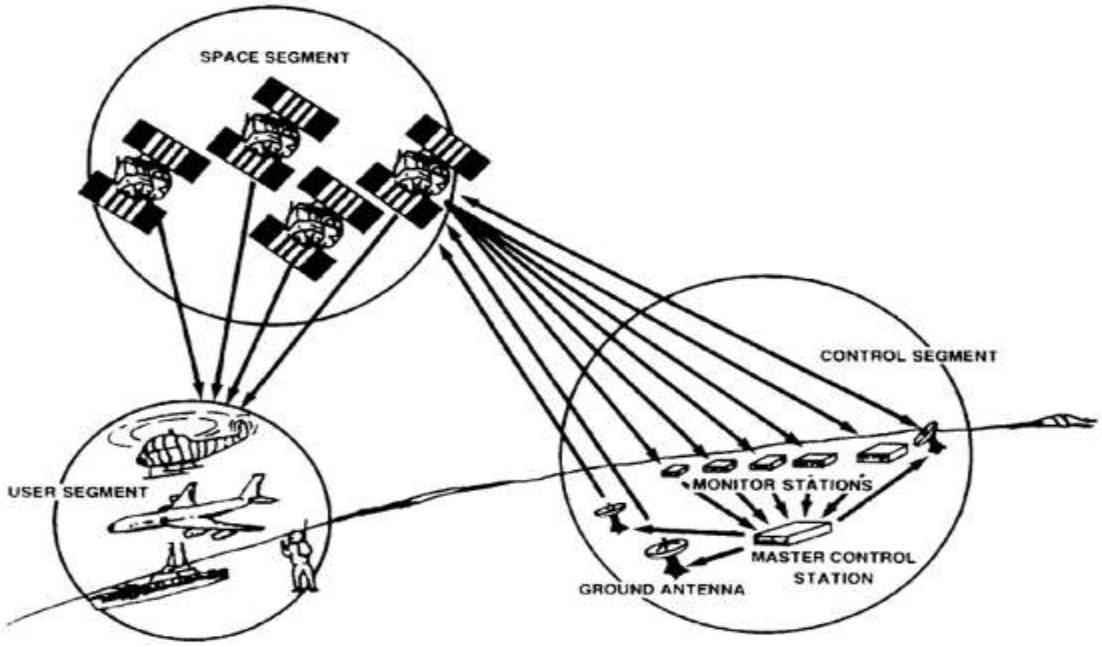

Figure 2.1: GPS segments (http://ucspace.canberra.edu.au/display/~s651224/GPS)

2.2.1 GPS Segments

The space segment consists of satellites. The satellites transmit signals controlled by atomic clocks. All the GPS satellites have a unique code called Pseudo Random Number (PRN). These codes are modulated with carrier frequencies. GPS satellites also transmit a navigation message with the carrier frequencies. Carriers and codes are used to determine distances from receivers to satellites and navigation message contains the coordinates of the satellites as a function of time *(El-Rabbany, 2002).*

The control segment of GPS is a worldwide network of tracking stations with a master controlling station. Right now there are five ground monitoring stations with receivers tracking the satellites, monitoring satellite health, computing orbital and clock data. The master controlling station is where the tracking data are processed in order to compute the satellite ephemerides and satellite clock corrections. It is also the station that initiates all operations of the space segment, such as spacecraft maneuvering, signal encryption, satellite clock-keeping, etc *(Rizos, 1999).* Satellite orbit and clock corrections are then uplinked to the satellite from three upload stations.

Having a GPS receiver in hand any one can enter in this segment. The GPS user segment includes all military and civil users. A receiver receives GPS signal that includes orbit information, clock corrections and atmospheric delay parameters. The receiver detects position of the satellites for a given moment and processes the received signal in order to determine the position of the user.

2.2.2 GPS Satellite Constellation

There are 32 satellites operating for global navigation. GPS satellite orbits are more or less circular and have an inclination of 55^0. The 24 satellites are deployed in six orbital planes containing four each to ensure that at least *four* satellites are visible from any unobstructed site on the earth surface. However, from the GPS constellation geometry, four to ten satellites will be visible from anywhere in the world if minimum elevation angle 10^0 is considered *(El-Rabbany, 2002).*

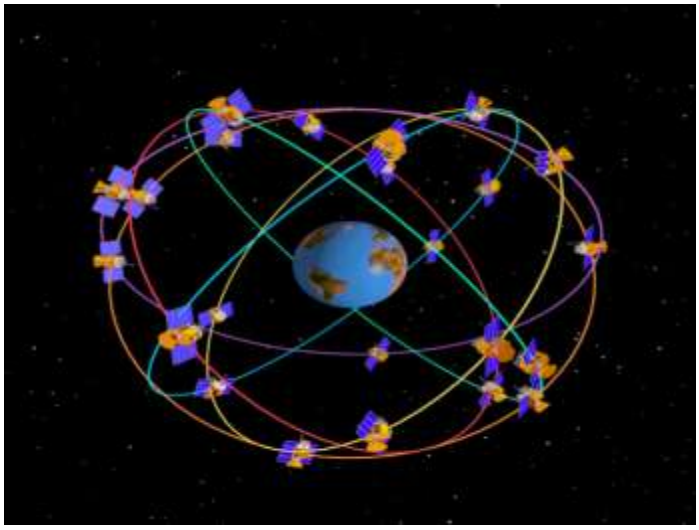

Figure 2.2: GPS satellite constellation

The Satellite antennas are directed toward earth center. Block II/IIA GPS satellites carry four onboard atomic clocks, two cesium (Cs) and two rubidium (Rb) where as IIR satellites carry three rubidium clocks.

2.2.3 GPS Signals

Two *L* band frequencies are used for GPS code and navigation message broadcasting. Multiplying 154 and 120 to the fundamental frequency f_o (10.23 MHz), yields two microwave carrier waves *L1* and *L2* respectively. The frequencies of the two carrier waves are: $f_{L1} = f_o \times 154$ =1575.42 MHz, and $f_{L2} = f_o \times 120$ = 1227.6 MHz *(Rizos, 1999*). The uplink frequency to the satellite is 1783.74 MHz.

GPS has two basic code schemes. These are called the 'Course Acquisation Code (C/A- code)' and the 'Precise Positioning Code (P- code)'. The P code is encrypted through modulation by a further secret code (the W- code) to produce a new 'Y- code'. Both carrier signals contain the navigation message *(Rizos, 1999).* The C/A- code is modulated with *L1* and the P- code is modulated with both *L1* and *L2* carrier frequencies. From 2005 the C/A- code is also transmitted through *L2* carrier frequency known as *L2C*.

	C/A- Code	**P- Code**
Chip rate	1.023 Hz	$10.23 \cdot 10^6$ Hz
Chip length	≈ 300 m	$\approx 30\ m$
Repetition time	Millisecond	One week
Code type	37 unique code	37 one week segments
Properties	Easy to acquire	More accurate

Table 2.2: C/A and P- code at a glance

2.2.4 Pseudo Random Number

The Pseudo Random Number (PRN) is a binary code modulated on the GPS carrier frequency. It is generated from a number between 1 to 37. Each satellite has a unique PRN code. The C/A, P-codes are example of the PRN.

2.2.5 The Pseudo Range Measurements

The PRN codes are accurate time marks that permit the receiver's navigation computer to determine the time of transmission for any portion of the satellite signal *(Rizos, 1999).* The receiver also knows time of the received signal. Computing the time difference between a GPS signal transmission and reception the GNSS receiver measures the distance between satellite and receiver. Mathematically the pseudo range can be expressed as,

$$P_k^p = (T_k - T_j)c \qquad 2.1$$

Where, T_k and T_j denote the receiver clock and the satellite signal transmission time. In a more precise way, the pseudo range:

$$P_k^p = \rho k + (\Delta T_k - \Delta T_j)C + I + Z \qquad 2.2$$

Where, ρk is the true range, receiver and satellite clock corrections are denoted by ΔT_k, ΔT_j respectively and ionospheric and tropospheric delays are represented by *I* and *Z* respectively.

2.2.6 The Carrier Phase Measurements

The wavelengths of the carrier waves *(19 cm for L1 and 24 cm for L2)* are much shorter than the C/A and P- code chip length, *see Table 2.2*. Assuming a measurement resolution of 1-2% of the

wavelength, this means that carrier phase can be measured to millimeter precision compared with a few meters for C/A code measurements *(Rizos, 1999).* This particular GPS observable is the phase of the received carrier with respect to the phase generated in the GNSS receiver. The difference between received carrier phase and receiver generated phase is called the carrier beat phase or beat frequency caused by Doppler effect. The phase measurement range is between 0° to 360°. The phase measurement observations can be described according to *Teunissen and Kleusberg (1998)* as:

$$\lambda_0 \Phi_A^j = \rho_A^j + c(\tau_A - \tau^j) + Z_A^j - I_A^j + \lambda_0 N_A^j + \epsilon \quad 2.3$$

Where, subscript j denotes satellite and A denotes receiver. In the *Equation 2.3,* λ_0 is the wavelength of the carrier and Φ_A^j is the carrier phase in cycles, the delay caused by troposphere Z_A^j, the ionospheric delay I_A^j , the phase ambiguity N_A^j, and other error sources ϵ (i.e. multipath, other noise sources)

One obvious problem with carrier phase measurement is that it is ambiguous as the GNSS receiver is unable to distinguish between wavelengths of carriers.

2.2.7 GPS Point Positioning

Point positioning mode applies to a single receiver for determining its position. The receiver tracks satellites for determining its position. For point positioning minimum four satellites are required to determine receiver co-ordinates with respect to the earth's center. Satellite coordinates and range are needed, that receiver gets from navigation message and pseudo-range measurement. The satellite and receiver clock error has an effect on range measurement. However, satellite clock error is corrected by navigation message. Whereas receiver clock error is still unknown. Therefore, there are total four unknowns that have to be determined, three co-ordinates and a receiver clock correction. That is why minimum four satellites are required to determine receiver position. If more than four satellites are tracked, either a least square estimation or a Kalman filtering technique is applied *(El-Rabbany, 2003).*

2.2.8 Single Differencing

Let, L_A^jbe the carrier phase measurement for a station A and L_B^j the carrier phase measurement of station B. Then from *Equation 2.3* we have:

$$L_A^j = \rho_A^j + c(\tau_A - \tau^j) + Z_A^j - I_A^j + B_A^j \quad 2.4$$

$$L_B^j = \rho_B^j + c(\tau_B - \tau^j) + Z_B^j - I_B^j + B_B^j \quad 2.5$$

Where, the observed carrier phase measurements are $L_k^j = \lambda_0 \Phi_k^j$ and the phase ambiguities are $B_k^j = \lambda_0 N_k^j$. Now we take the difference between *Equation 2.4* and *Equation 2.5*. Thus the single difference phase for epoch *t* is then:

$$\Delta L_{AB}^j(t) = \Delta\rho_{AB}^j(t) + c\Delta\tau_{AB}(t) + \Delta Z_{AB}^j(t) - \Delta I_{AB}^j(t) + \Delta B_{AB}^j \quad 2.6$$

If the receivers are close to each other then the differential trophospheric and differential ionospheric terms cancel out and the equation becomes simpler. So, here we have the single differencing equation:

$$\Delta L_{AB}^j(t) = \Delta\rho_{AB}^j(t) + c\Delta\tau_{AB}(t) + \Delta B_{AB}^j \quad 2.7$$

Equation 2.7 can be expanded and expressed in a local coordinate system using azimuth, α and elevation, ε for each satellite according to:

$$\Delta\rho_{AB}^j(t) = \Delta e \sin\alpha^j \cos\varepsilon^j + \Delta n \cos\alpha^j \cos\varepsilon^j + \Delta v \sin\varepsilon^j \quad 2.8$$

Where, the east, the north and the vertical components of the baseline between the two receivers are Δe, Δn and Δv respectively.

2.2.9 GPS Error sources

There are a number of error sources that causes degradation of GPS measurements. In order to get better accuracy these error sources must be sorted out and corrected.

Due to the gravitational forces there is a possibility of slight shift in satellite orbits even though they are deployed in the orbital planes very precisely. However, orbital data are controlled and corrected in the control segment and are sent to the receivers. The receiver gets this correction as ephemeris data. Due to orbital error accuracy could very more or less 2 meters.

The satellites and receivers both carry clocks but the inaccuracy in the time between the transmitting satellite's clock and the receiver clock can lead to a major problem called clock error. Despite the synchronization of the receiver clock and satellite clock during position determination, the remaining inaccuracy of the time still leads to an error about 2 meters, *see The GPS System (2009)*. To get rid of this problem single and double differencing can be an ideal option.

When satellite signals are reflected by any objects it causes multipath error. For GPS signals this effect mainly appears in the neighborhood of large buildings or other elevations. The reflected signal takes more time to reach the receiver than the direct signal. The resulting error typically lies in the range of a few meters, *see The GPS System (2009).*

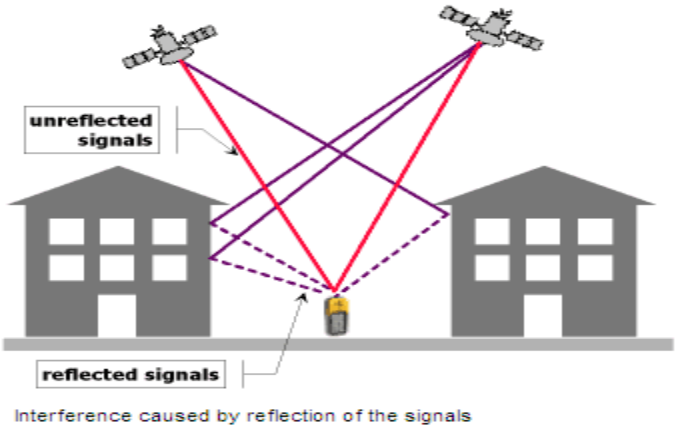

Figure 2.4: Multipath effect, see The GPS System (2009)

The earth atmosphere causes delays to the propagating radio wave. Outside the earth atmosphere the radio wave travels at a speed of light but when it propagates through earth atmosphere then it slows down. The ionosphere is full of free electrons and charged particles. This ionized layer of the atmosphere refracts the radio waves of the satellites. The effect of the ionosphere is frequency dependent. The delay is larger for lower frequencies. The ionospheric error can be mitigated by combining the two carriers linearly. Linear combination of *L1* and *L2* yields another frequency known as ionosphere free combination *Lc;*

$$Lc = 2.54 \cdot L1 - 1.54 \cdot L2 \qquad 2.9$$

Water vapor in the troposphere also delays the electromagnetic propagation. It has less effect in signal delay than the ionosphere. Higher elevation cutoff angle may reduce the tropospheric delay to some extent.

A phase ambiguity problem occurs when carrier phase measurement is concerned. The distance is measured by counting full cycles and adding fractional phase. However, the initial number of cycles is unknown. This unknown value is described as phase ambiguity and is different for different satellites and frequencies.

For uninterrupted observations the phase ambiguity is constant but when a signal blockage occurs a missing cycle is observed. This phenomena is called cycle slip and causes a new ambiguity. Cycle slip repair therefore restores the continuity of carrier cycle counts and ensures that there is only one ambiguity for each satellite-receiver pair, *see The GPS System (2009).*

The earth surface can cause errors in the positioning too. There are always different types of geophysical processes going inside earth crust (i.e. earthquake, ocean loading, solid earth tide, polar motion etc). However, these processes can be modeled and effects can be truncated.

2.3 Tilted GNSS Antenna Concerns

The GPS signal reception point inside a GNSS antenna is not homogeneous. The so-called electrical phase center varies with the direction of the incoming signal. Thus the Phase Center Variation (PCV) of a GNSS antenna can be described as a function of satellite elevation and azimuth. However, the PCV properties depend on the GNSS antenna type. Variations of the phase center can vary from millimeter to centimeter. So, if the PCV corrections are not taken into account during the GPS data processing then solutions can lead to errors from a fraction of a millimeter up to tens of centimeter. For a particular antenna type antenna the phase center can be modeled and corrections can be added during processing of GNSS data.

However, if the GNSS antenna is tilted then the scenario is more complicated and modeled absolute phase center corrections cannot be simply added during GPS data processing. Otherwise it might lead to a systematic error to the solutions. The PCV modeling of a tilted antenna depends on the observation type (i.e. static or kinematic) and the site location.

The GNSS measurements for this thesis work were conducted in an environment where the GNSS antenna rotated about the azimuth axis of the 20 meter radio telescope and tilted about the elevation axis. Consequently a phase center correction model was required, *see Chapter three* for more details.

CHAPTER THREE- GNSS ANTENNA PHASE CENTER CORRECTION

3.1 Phase Center Corrections for a Tilted GNSS Antenna

Usually absolute phase center corrections are applied in GNSS data analysis. The absolute phase corrections are for example provided by the IGS (International GNSS service) and are applicable for static measurements i.e. non-moving antennas. As the receiving antenna on top of the radio telescope is not pointing towards zenith but is moving with the VLBI radio telescope, we cannot use the standard IGS absolute antenna calibration files to correct for phase center variations. Hence we need to do the corrections directly in the RINEX files before the data processing

Figure 3.1 shows phase center variations in meters with respect to azimuth of the receiver antenna for different elevation. The phase center does not vary significantly due to azimuth. Therefore we have neglected satellite azimuth in our approach of correcting phase center variations. We focus mainly on the elevation dependency of the satellite and telescope antennas to find the true elevation of the satellite with respect to the tilted receiver antenna for a particular epoch.

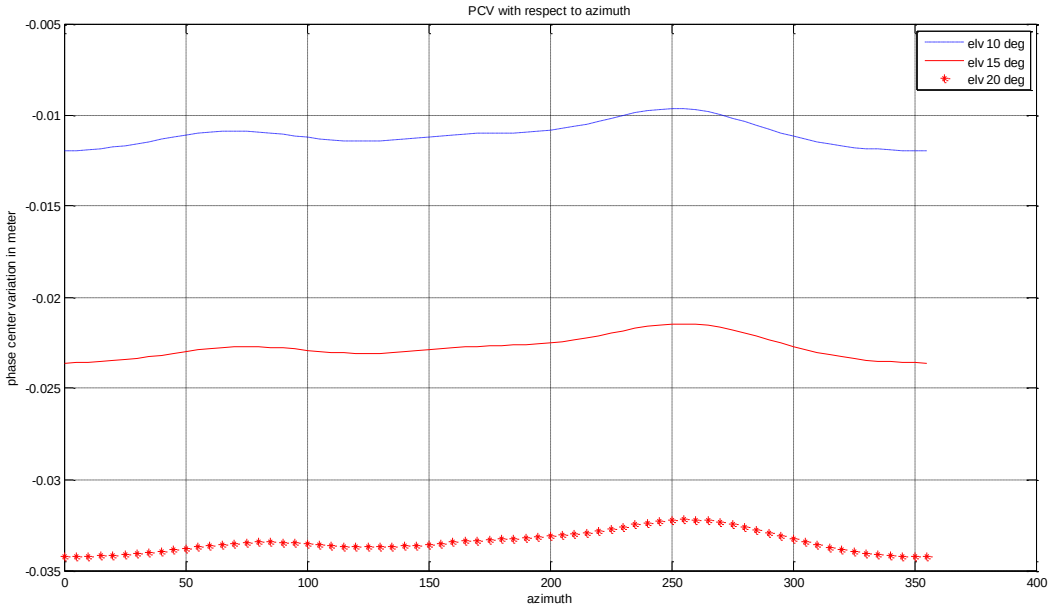

Figure 3.1: PCV with respect to azimuth

3.2 Satellite and Telescope Elevation

Satellite orbit data for a particular day can be downloaded from the IGS ftp sites. The satellite information is then extracted from a satellite ephemeris file. We have used satellite broadcast ephemeris files to extract azimuth and elevation of all satellites. The GPS satellites have altitude

around 20,000 km and broadcast ephemeris file has an uncertainty of 100 cm. This amount of uncertainty will not affect our result. The extracted elevation and azimuth of the satellites from the broadcast ephemeris are good enough for calculation of true elevation of the satellites with respect to tilted receiver antenna. A MATLAB program was written to give satellite elevation and azimuth angles for different satellites. This program out-puts angles as a function of time. For a particular epoch we have the elevation of all 32 satellites. Sampling rate of 1 sec was used to get satellite elevation for every second. *Table 3.1* shows an example of output of the program.

Sat/No Time	***1***	***2***	***3***	***4***	***5***	***6***	***……...***	***32***
1	12.3559	30.4564	-8.8975	-20.8974	60.8757	50.7876	……..	85.2343
2	12.4533	30.9878	-8.8676	-20.8643	60.9223	50.5328	……..	85.3697
3	13.5743	31.5349	-7.3423	-19.6432	61.0976	50.4635	……..	85.1343
….	….	….	….	….	….	….	……..	….
3600	70.8786	-5.6453	46.9784	25.3453	-30.7867	-10.8643	……..	-65.6754

Table 3.1: Example of the satellite elevation table.

The first column of the table shows time in seconds where as the first row shows the satellite number. Elevation angles are given in degrees. Negative numbers represent that the satellite is not visible for that particular epoch. We can set the observation time in the program. For instance if we want to get satellite elevation angles from UTC 16:00 hrs to UTC 17:00 then all we have do is to set the observation start time at 16:00:00 hrs and set the observation time 3600 seconds.

Telescope azimuth and elevation angles were noted during the ordinary VLBI and GNSS sessions.

3.3 True Elevation of the Satellite With Respect to the Tilted GNSS Antenna

The receiver antenna mounted on the top of the radio telescope is always moving during VLBI and GNSS sessions. Thus the elevation angle of the satellite seen from the GNSS antenna varies. The true elevation is the angle of the satellite seen from the GNSS antenna.

The true elevation is highly dependent on the telescope azimuth. The position of the GNSS antenna drastically changes with the VLBI radio telescope azimuth. For instance if the radio telescope rotates by 180 degrees then the GNSS antenna would face completely opposite to the previous position and satellite visibility could be totally blocked. *Figure 3.2* shows the actual angle of the satellite as seen from the GNSS antenna.

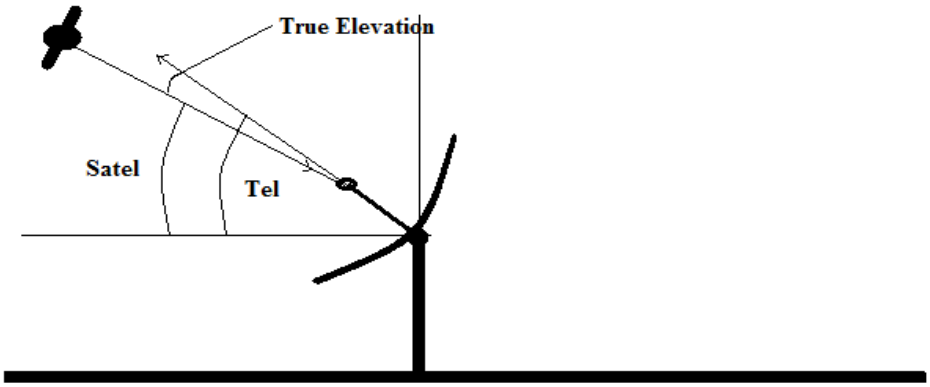

Figure 3.2: True elevation

$$\varepsilon_t = \ (90 - Satel) - \cos(\alpha) \cdot (90 - Tel) \qquad 3.1$$

Where, ε_t = True elevation, $Satel$ = satellite elevation, α = telescope azimuth, Tel = telescope elevation.

In *Equation 3.1* the satellite and telescope elevation angles are 90 degrees subtracted value from the satellite and telescope elevation table. When the satellite elevation is greater than 90 then the value considered as not a number (NaN) since the satellite is not visible. The telescope azimuth determines the position of the receiving antenna from where true elevation has to be calculated. *Table 3.2* illustrates an example of true elevation table. The first column in the table shows start and end time (UTC) of the observation. Column two to thirty three is the satellite number. 'NaN' represents that the satellite is not visible of the satellite at that particular time.

1	**2**	**3**	**4**	**5**	**6**	**7**	**8**	**……**	**33**
72000	NaN	NaN	24	11	NaN	5	10	…….	85
72001	NaN	NaN	24	11	NaN	5	11	…….	85
72002	NaN	NaN	23	10	NaN	4	11	…….	84
72003	NaN	NaN	23	10	NaN	4	11	…….	84
72004	NaN	NaN	23	10	NaN	4	11	…….	84
….	….	….	….	….	….	….	….	…….	….
75600	15	30	NaN	NaN	4	90	78	…….	NaN

Table 3.2: Example of the true elevation table

3.4 IGS Antex File for PCV

Absolute antenna phase center correction files can be downloaded from:

ftp://sideshow.jpl.nasa.gov/pub/gipsy_files/gipsy_params/antenna_cals_xmit

The antex2xyz.py script was used to create an antenna calibration file with elevation step of 1 degree and azimuth step of 5 degree. However we are mainly concerned about elevation dependency therefore azimuth is not of an importance. The elevation dependent phase center

correction table for each elevation angle when azimuth is 180 degree was created. The correction values were then taken for each elevation angle when azimuth is 180 degree because at 180 degree the corrections are almost equivalent to the average value. All correction values are in millimeters. Thus all the corrections were converted into cycles for *L1, L2* and in meter for *P1, P2* observables. No corrections were done for *C1* observable since in the 'antex' file there was no correction of phase center variations for C/A code measurements. Only *L1, L2, P1, P2* and ionosphere free corrections are available.

3.5 Correction of RINEX File

A java program has been written to do the correction of RINEX data. The necessary Input files for this program are generated by the written MATLAB program. We get the true elevation angle table from the MATLAB program, which was saved as '.xls' file and later converted into java readable '.csv' file delimited by '#'. Another input file is the elevation dependent phase center correction table which is downloaded from the IGS site. This was also converted into '.csv' file delimited by '#'.

The software consists of three different packages which are 'data_handler', 'elevation_correction', file_handler following the 3-stage architecture. The top tier of the software is the 'elevation_correction' package which has a single class named 'Elevation_Correction.java'. This class has the main method to execute the program. The main method takes three arguments: first one being the true elevation angle with respect to time. The second argument is the elevation dependent phase centered correction table. The third argument is the RINEX data file.

The third tier of the software is the 'file handler' package which has two classes 'FWriter.java' and 'FileEditor.java'. These two classes handle the files taken as argument by the main method.

The 'FileEditor.java' is a simple class that initiates file reading objects. The 'FileWriter.java' is a class that creates a similar data file in the same directory as the RINEX data file. The new data file is named as the original data file with a 'crctd' prefixed to it.

The middle tier of the software is the 'elevation_correction' package which has four different classes named 'Satellite.java', 'SatelliteData.java', 'SatelliteTime.java' and 'DataFixer.java'.

The 'Satellite.java' is the object that simulates all corrections i.e. L1 L2 P1 P2 for each visible satellite in the RINEX data file. The 'DataFixer.java' reads the RINEX file and creates 'Satellite' objects based on the information from a specific line. The 'Satellite' objects are added to a list and passed to the 'SatelliteData.java' object from the list. The 'SatelliteData.java' object has methods to perform the correction of the data. Once the 'SatelliteData.java' object corrects the data for a single satellite, the 'DataFixer.java' object then writes the data to the corrected file. The 'SatelliteTime.java' object keeps tracking of the elapsed time.

The execution of the software is pretty simple. If Java is not installed then Java has to be installed in the computer. After installation run the software in the format shown below. The software is a '.jar' file.

'Java – jar (location of the .jar file) location of the true elevation angle table (.csv file) location of the phase center correction table (.csv file) location of the input RINEX file'

3.6 Analyzing Corrected RINEX File

The software generates phase center corrected RINEX data file. The new corrected file is exactly in the same format as the original RINEX file. To check this, the corrected RINEX file was converted in to 'Hatanaka' format and then back converted in to RINEX format. Successful conversion ensures that new edited file is not corrupted. However, the corrected file is then used for processing in the *GIPSY OASIS version 5.0 (Webb and Zumberge, 1993)* to realize the effect of correction.

We do not expect to have a drastic change in the result because our original file is noise affected. The radome around the radio telescope causes a huge amount of multipath which corrupts the GNSS observations. *Figure 3.3* is the quality check result of the original RINEX file. This GPS observation was done during the seventh day of July in the year 2010 with an *ASHTECH UZ-12* receiver. The quality check of the RINEX file was done using '*teqc'* software (*http://facility.unavco.org/software/teqc/teqc.html*)

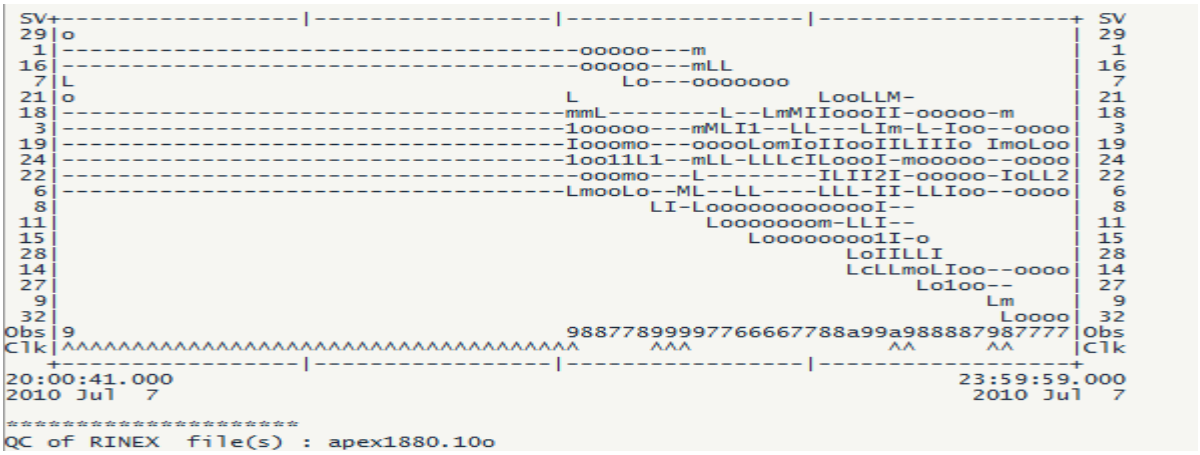

Figure 3.3: quality check of an original RINEX file

Symbol codes for 'SV':

(hierarchy is left-to-right, top-to_bottom)

C receiver clock slip m n-msec multipath jump

I ionospheric phase slip M MP1 and MP2 slips

1 multipath MP1 slip only 2 multipath MP2 slip only

- (lite) missing data epoch(s) L Bit 0 of LLI set (rx lost lock)

. no A/S; C/A c no A/S; L1 C/A

: no A/S; L1 P1 = L1 C/A L2C

~ no A/S; L1 C/A L2 P2 * no A/S; L1 P1 L2 P2

, A/S on; C/A a A/S on; L1 C/A

; A/S on; L1 P1 e L1 C/A L2 L2C

o A/S on; L1 C/A|P1 L2 P2 y A/S on; L1 P1 L2 P2

note: 'no A/S' == GPS antispoofing off or unknown, or not GPS SV

From the figure we see that our original file does not contain quality observations. The data file is highly corrupted by missing epochs, multipath jumps and other error sources. After processing of original and corrected files we have tried to compare their residual plots. The plots look almost identical because the changes due to the correction is very little than the effect of noise. However there are changes in the observations from fraction of a millimeter to few tens of centimeters after correction. *Figure 3.4* shows the residual plot of the original RINEX file and the corrected RINEX file. The PCV correction model was applied to the original RINEX file from 22:00 hours to 23.59:59 hours and the impact of corrections were observed.

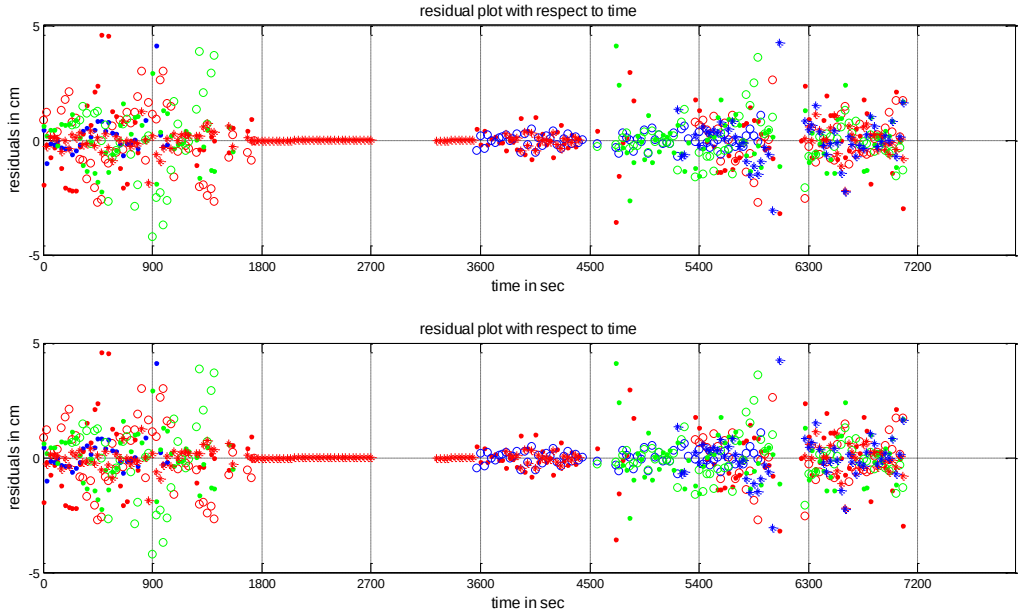

Figure 3.4: Post processing residual plots of the RINEX file before (top) and after correction (bottom)

Differences of residuals vary within a fraction of a centimeter. However, in very few cases they differ more than couple of centimeters. And higher differences were occurring in a regular interval this might be due to the telescope motion. The radio telescope was changing its position in every 15 minutes. *Figure 3.5* is a difference plot of residuals between corrected and original RINEX file after processing.

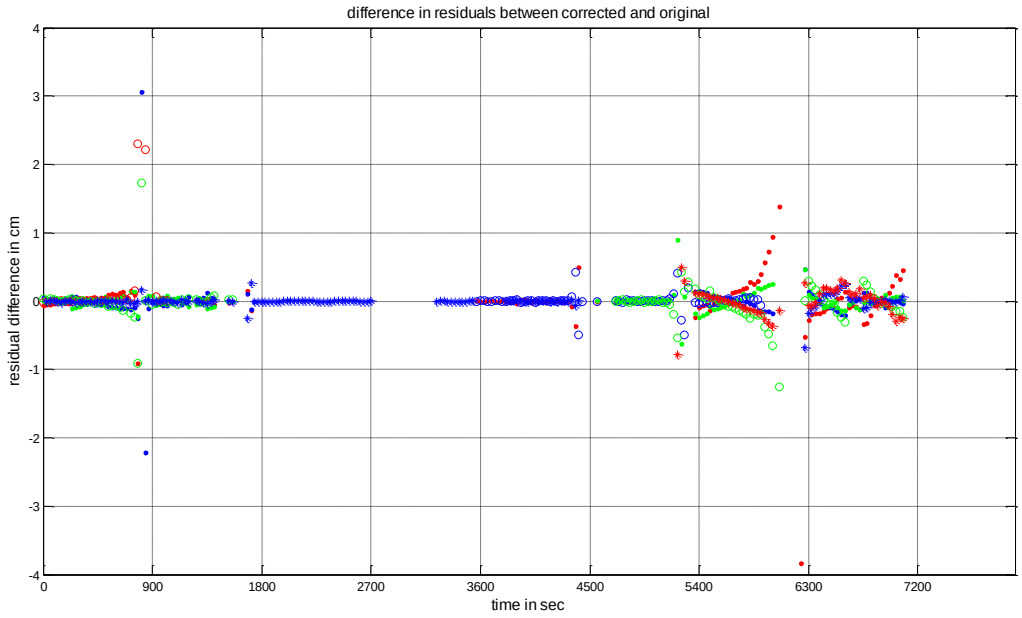

Figure 3.5: Post processing residual difference between corrected and original RINEX file

3.7 Conclusion

This PCV correction model was applied to several GNSS observation files. Unfortunately, it was not possible to distinguish the effect of the PCV corrections. All the observation files were badly corrupted and several data were missing, *see section-3.6* and the possible reason could be the environment inside the radome was very noisy and/or the receiver quality was bad. However, in the December 2010 the old receiver was replaced by a new *LEICA GRX1200* receiver.

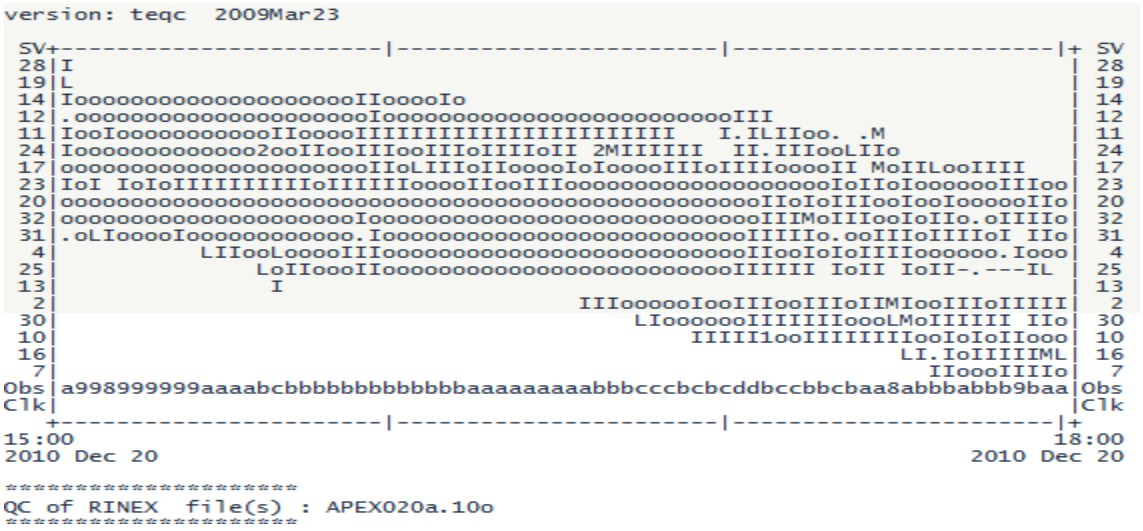

Figure 3.6: Quality check of the GNSS data collected by a LEICA GRX1200 receiver

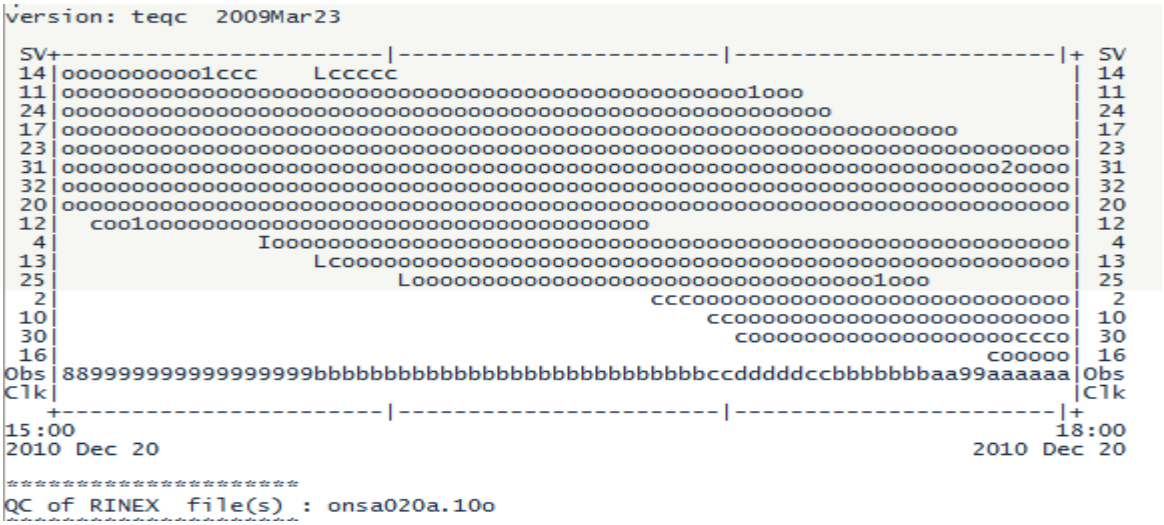

Figure 3.7: Quality check of the GNSS data collected from nearby ONSA station

Figure 3.6 and *Figure 3.7* is a visual comparison of the observed data quality. For symbol meaning please *see section-3.6*. The new receiver data are suffering from very high amount of phase ambiguities. However, taking the data quality of the GNSS observations into account the new PCV correction model was not applied for the further steps of the thesis.

CHAPTER FOUR- GNSS DATA COLLECTION AND ANALYSIS

4.1 Field Data Collection

An AT504 Leica choke ring antenna has been installed top of the 20 meter radio telescope for acquisition of GPS data *(Bergstrand et al., 2000).* GNSS data were collected during different VLBI sessions and dedicated GNSS observation sessions. Three types of receivers were used and the data quality was compared. However, it was not possible to use 2001, 2002, 2008 data for measuring reference point of the radio telescope due to unavailability of high rate clock in GPS product archives.

The protecting radome of the 20 meter radio telescope often restricts satellite visibility and results in poor data quality. Error sources such as multipath, lower elevation angle, shadowing effects of telescope azimuth angle, phase center variations increase noise level of the environment inside the radome to a large extent. However, a good quality receiver is required for this particular case. A quality receiver can minimize noise in observation data. However, the IGS station at Onsala Space Observatory was taken as reference station and collected field GNSS data were then compared with the reference station data. The single differencing method was used to do the comparison. An in-house MATLAB software was used to carry out single differencing technique. We expect to have observations with long arcs without discontinuity and cycle slips. However, discontinuities are expected when the radio telescope is pointing towards North and if the elevation angle is low. *Table 4.1* shows GNSS data available for the 20 meter radio telescope reference point determination.

Session Name	Day of Observation	Session Type	Data Rate	Receiver Type
APEX_100630	2010-06-30	GNSS	1Hz	ASHTECH UZ-12
APEX_100701	2010-07-01	GNSS	1Hz	ASHTECH UZ-12
APEX_100707	2010-07-07	GNSS	1Hz	ASHTECH UZ-12
APEX_EUR.106	2010-07-05	VLBI	1Hz	ASHTECH UZ-12
APEX_RD1005	2010-06-29	VLBI	1Hz	ASHTECH UZ-12
APEX_R1438	2010-07-06	VLBI	1Hz	ASHTECH UZ-12
APEX_R1462	2010-12-20	VLBI	1Hz	LEICA GRX1200
APEX_EUR.109	2011-01-17	VLBI	1Hz	LEICA GRX1200
APEX_110223	2011-02-23	GNSS	1Hz	LEICA GRX1200
APEX_110224	2011-02-24	GNSS	1Hz	LEICA GRX1200
APEX_110226	2011-02-26	GNSS	1Hz	LEICA GRX1200
APEX_110227	2011-02-27	GNSS	1Hz	LEICA GRX1200
APEX_R1471	2011-02-21	VLBI	1Hz	LEICA GRX1200
APEX_RD1101	2011-02-22	VLBI	1Hz	LEICA GRX1200
GPS_110322	2011-03-22	GNSS	1Hz	LEICA GRX1200
GPS_110324	2011-03-24	GNSS	1Hz	LEICA GRX1200
APEX_EUR110	2011-03-23	VLBI	1Hz	LEICA GRX1200
APEX_R1476	2011-03-28	VLBI	1Hz	LEICA GRX1200
APEX_RD1102	2011-03-29	VLBI	1Hz	LEICA GRX1200

Table 4.1: GNSS observation list

4.2 Receiver Type: ASHTECH UZ-12

An ASHTECH UZ-12 receiver was used to collect GNSS data during CONT08 VLBI sessions in the year 2008 and also VLBI and GNSS observations done in the year 2010. This very receiver is quite an old one and data collected using this receiver was not satisfactory at all. *Figure 4.1* shows an example of data quality of an ordinary VLBI session for day 180 in the year 2010. This figure shows *L1* and *L2* phase observations for both the IGS (left) and the field station (right). The field data quality was not good enough compared to the IGS station. Thus we cannot expect a good result from the data sets collected using this receiver.

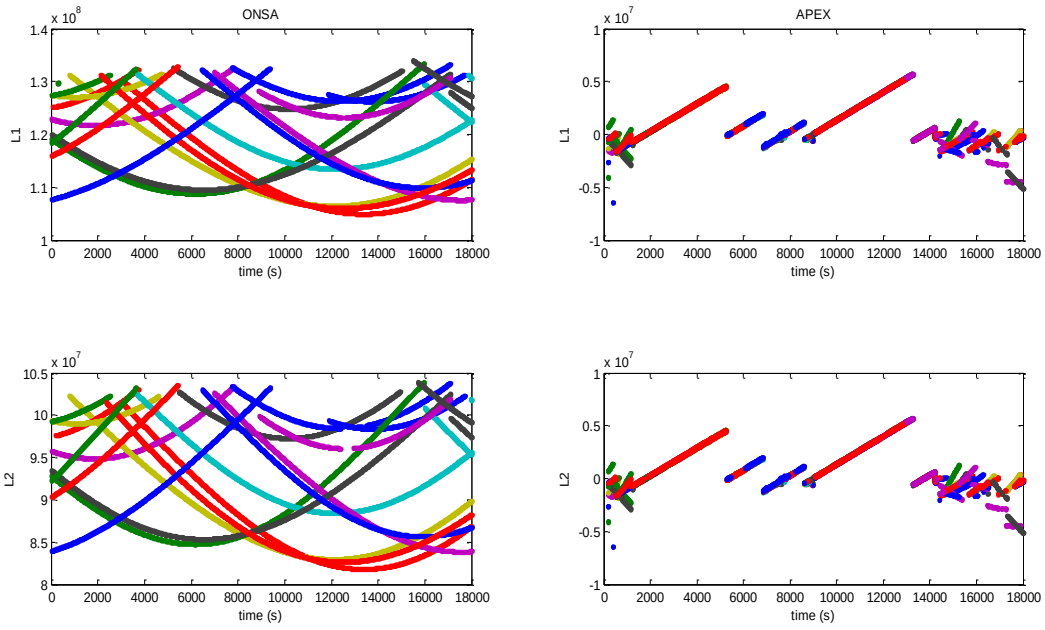

Figure 4.1: Phase observations of the IGS (left) and field (right) station, duration 5 hours (19:00:00 to 23:59:59). L1 and L2 observations are in cycles.

4.3 Receiver type: LEICA GRX1200

As shown in the previous section data collected using the receiver ASHTECH UZ-12 did not give satisfactory results. Therefore these GNSS data sets cannot be used for further processing. The ASHTECH UZ-12 receiver was replaced with a new LEICA GRX1200+ series. On 20th December a new set of GNSS data was collected during the R1462 VLBI session. *Figure 4.2a* shows the improvement of data quality and its compatibility with the ONSA station. *Figure 4.2b* shows the single differencing of the phase observations between the IGS and field station. However some small period of discontinuities are found and these may be a result of antenna motion or signal restriction due to azimuth and elevation of the telescope.

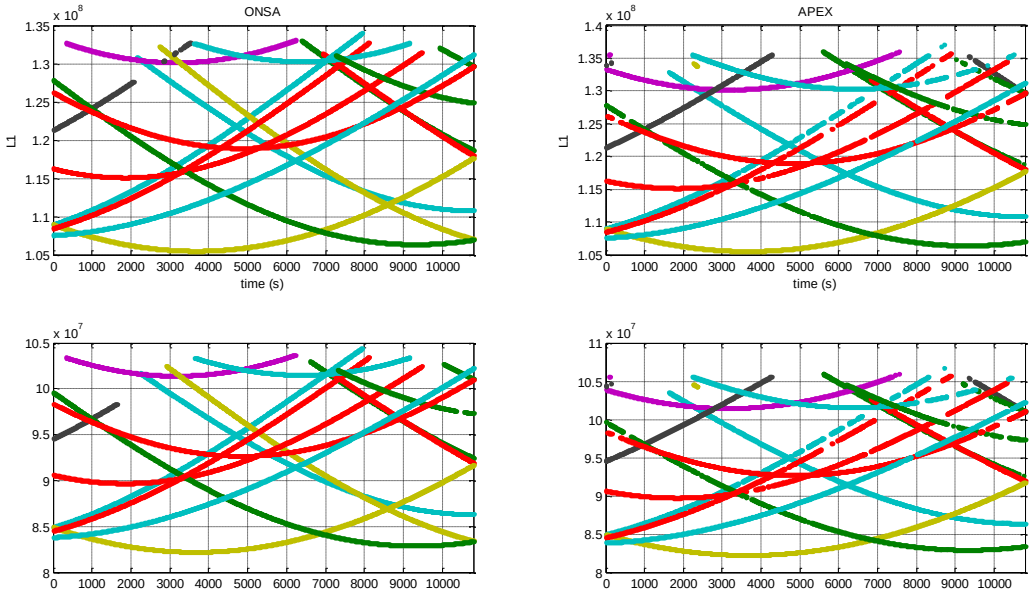

Figure 4.2a: Phase observations of the IGS (left) and field (right) station, duration 3 hours (15:00 to18:00). L1 and L2 phase observations are in cycles

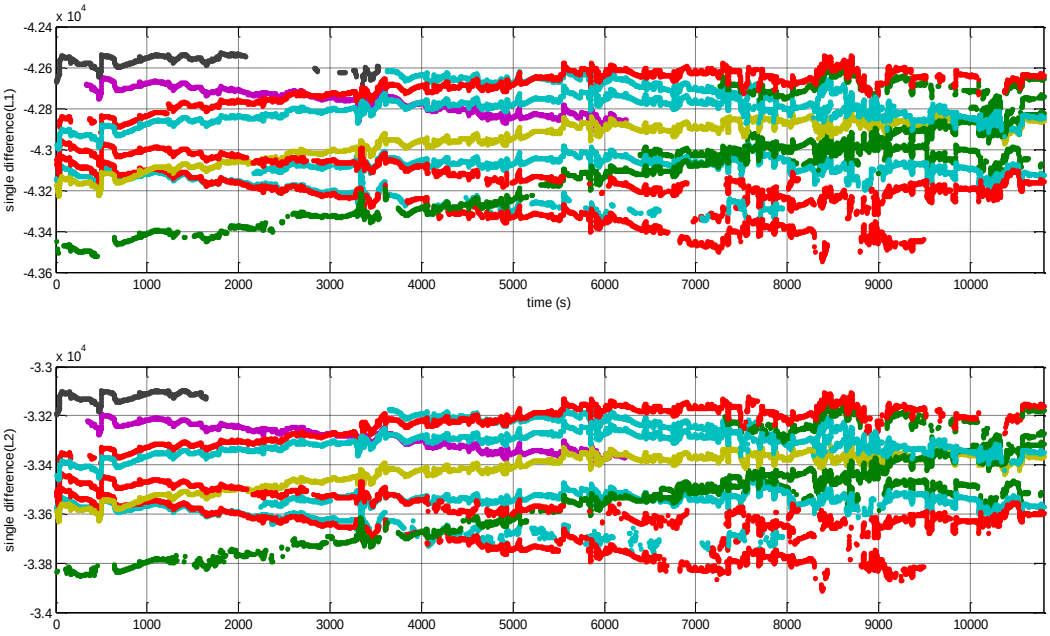

Figure 4.2b: Single differencing of phase observations (L1 & L2) between IGS and field station L1 and L2. Phase observations are in cycles.

We are already aware of the multipath effect in our site. The protecting radome of the 20 meter radio telescope causes severe multipath problems in GNSS data reception. Besides that the telescope dish blocks GNSS signals as well, which causes satellite invisibility. So we do not expect to acquire very good GNSS data sets. Signal to noise ratio (SNR) can give us indication about the multipath effect at the receiving end. *Figure 4.3* illustrates SNR inside the radome as a function of time. Fifteen hours of observation are shown. The observation starts at 00.00 hours day 082 in the year 2011and stops at 14:59:59 hours. During this time the telescope was positioned in thirty different positions with eight different elevation angles (i.e. 85, 80, 70, 60, 55, 45, 40 and 30). *Figure 4.3* shows that environment is very noisy. There were few satellites always maintaining a good SNR and others are between 30 to 45 dB. However we could still work with these data sets. *Figure 4.4* is the representation of the SNR as a function of the satellite elevation angle and *Figure 4.5* illustrates the SNR as a function of true elevation. However, it is quite difficult to interpret *Figure 4.4* and *Figure 4.5* in order to describe the actual condition of the environment inside the protecting radome.

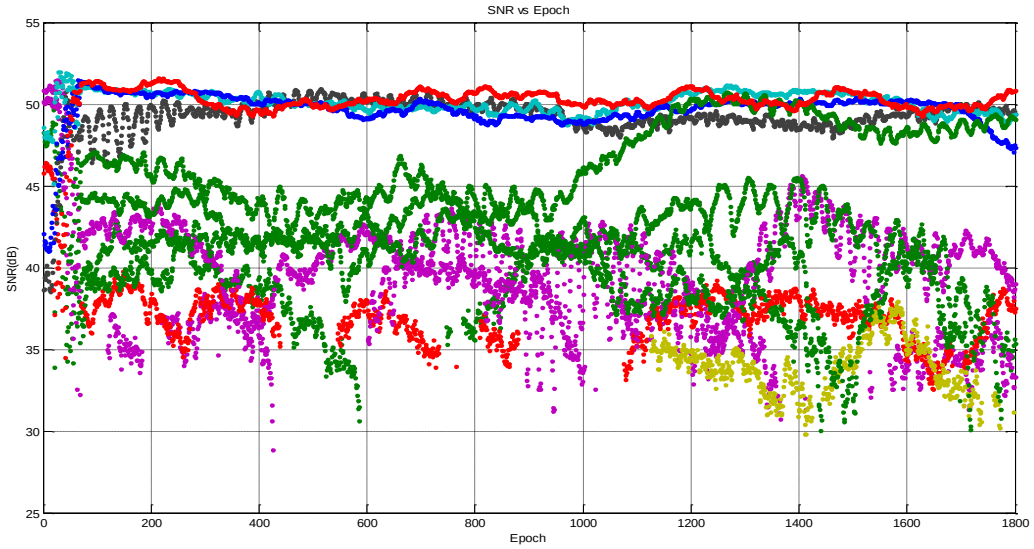

Figure 4.3: Signal to Noise Ratio at the receiving end

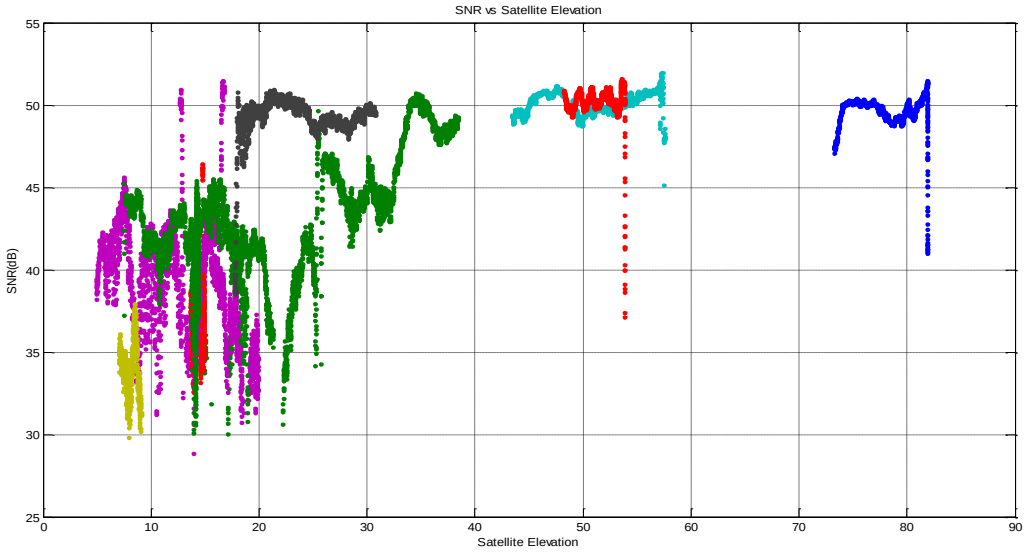

Figure 4.4: Signal to Noise Ratio as a function of satellite elevation

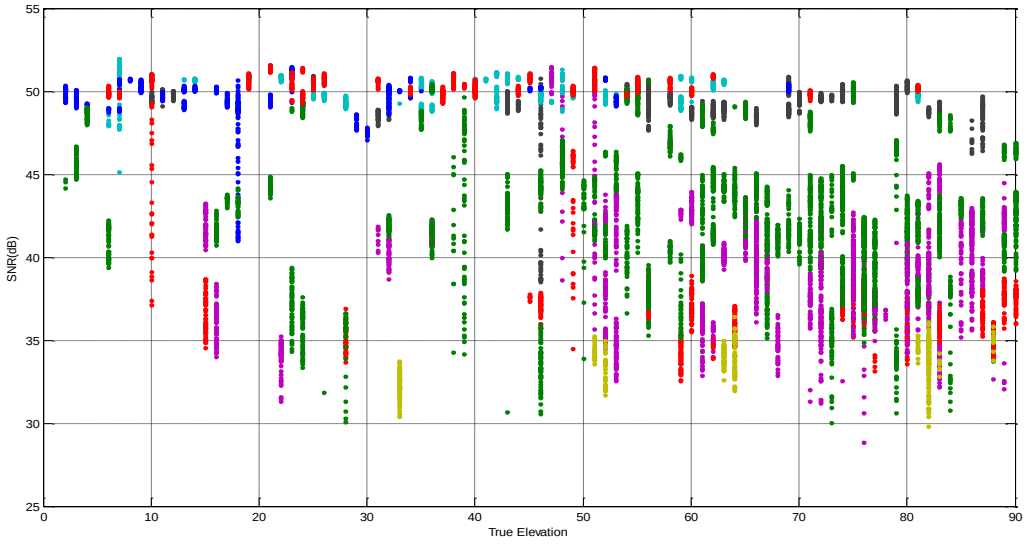

Figure 4.5: Signal to Noise Ratio as a function of true elevation

Signal to Noise Ratio with respect to the radio telescope elevation and azimuth are also shown below;

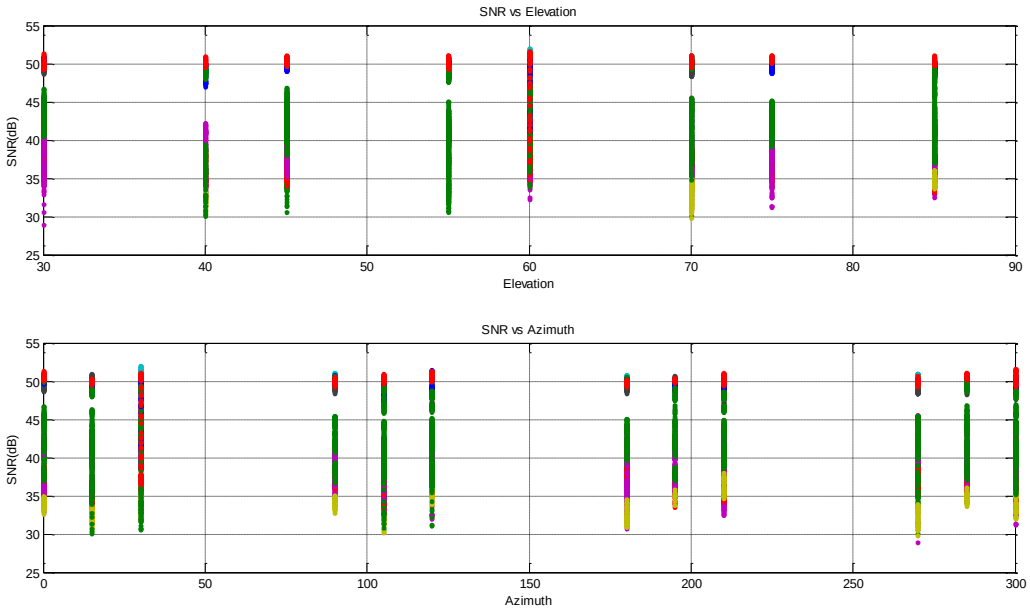

Figure 4.6: SNR with respect to elevation (top) and azimuth (bottom)

4.4 Data Processing Software

The raw data obtained from GNSS observations are in RINEX format which then processed using different data processing software. At Onsala Space Observatory there are different types of GNSS data processing software available, such as GIPSY OASIS *(Webb and Zumberge, 1993)* Bernese GPS software *(Dach et al. 2007).* In this project, the Jet Propulsion Laboratory (JPL) developed GIPSY OASIS V 5.0 was used considering the precise point positioning fact in kinematic mode. In-house MATLAB software *(Löfgren, 2011)* for GPS data processing has also been used. This MATLAB software was used to derive single differencing of the phase observations between the IGS and field station and to compare receiver performance, measuring signal to noise ratio and also used to derive satellite azimuth and elevation angles for PCV correction software.

4.4.1 GIPSY OASIS V 5.0

The GPS Inferred Positioning System – Orbit Analysis and Simulation Software or GIPSY-OASIS (GOA) is a software package developed by Jet Propulsion Laboratory at California Institute of Technology, USA *(Zumberge et al., 1997).* The software uses a Kalman filtering method to process GNSS data. A block diagram of the processing technique of this software is shown below. The GIPSY OASIS v5.0 was used to process GPS data both in kinematic and static mode for this project.

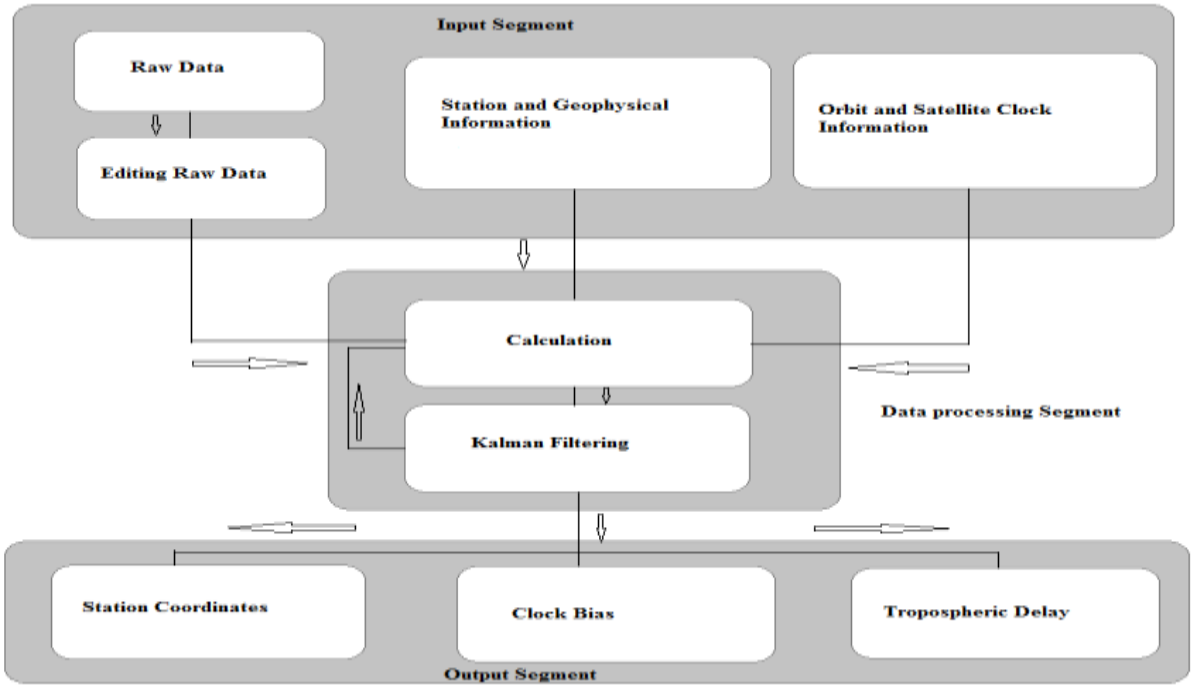

Figure 4.7: Block diagram of data processing segments of GIPSY OASIS software

4.4.2 In-house GPS Software

The in-house GPS relative positioning software was developed in MATLAB during 2009-2010 and still under development. This software is based on standard geodetic processing with single differences (*Equation 2.7*) current version of the software uses *L1* frequency together with satellite broadcast ephemeris (accuracy $\sim 100\ cm$) provided by IGS *(Löfgren, 2011*). Unlike GIPSY OASIS, this in-house GPS software uses a least squares method for data analysis. However, antenna phase center corrections are yet to add in the analysis. We have used this software to compare receiver quality with respect to the IGS station at Onsala Space Observatory through single differencing, as mentioned earlier, *see section-4.2, 4.3.*

4.5 Data Processing with GOA

The GNSS data were processed in kinematic mode with GOA. Stochastic random walk parameters were set precisely. An example of the *gd2p.pl* script is shown below.

```
#source  /opt/goa-5.0/rc_gipsy.csh

( /opt/goa-5.0/bin/gd2p.pl \

    -d \

    2011-03-23 \
```

-i ****

apex082a.11o \

-n ****

APEX \

-r ****

30 \

-type ****

k \

-add_ocnld ****

-tides ****

WahrK1 \

PolTid \

FreqDepLove \

OctTid \

OcnldCpn \

-trop_z_rw ****

5E-8 \

-wetzgrad ****

5E-9 \

-w_elmin ****

20 \

-post_wind ****

5.0E-3 \

5.0E-5 \

-orb_clk ****

flinnR \

-p ****

3370.60596216858 \

711.917567073841 \

5349.83079857581 \

-kin_sta_xyz \

13.5e-3 \

1.0e-3

30 \

RANDOMWALK \

> gd2p.log)

Geophysical model parameters and constrains were set as default. The type of processing mode in the *–type* flag was set in kinematic (i.e. *k*). The data processing rate was set to 30 sec. The post window range was 5 meters for code and 5 centimeter for phase measurement. Post window works as a filter in the data processing. The *'-p'* flag represents the priori position of the antenna. The stochastic random walk parameter was set in *'-kin_sta_xyz'* flag. The solution of the processing then can be found in the '*tdp_final'* file.

The coordinates were extracted from the *tdp_final* and plotted. *Figure 4.6* shows an example for the results of the GOA high rate kinematic analysis. The observation starts at 00.00 hours day 082 in the year 2011 and stops at 14.59:59 hours. The elevation angles of the radio telescope were low (i.e. 30, 45) from 02:00 hours to 06:00 hours. From the *Figure 4.8* it is clear that during this transition period (corresponding epochs 241 to 720), analysis of the coordinate solutions were distracted.

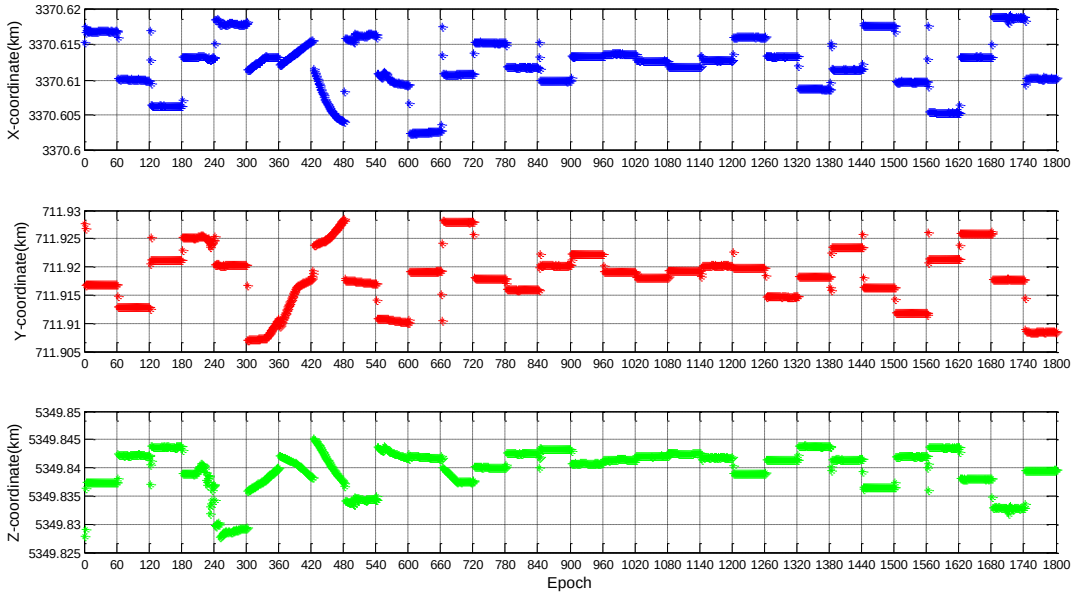

Figure 4.8: GOA high rate kinematic GNSS coordinate solution (March 23, 2011)

CHAPTER FIVE- POST PROCESSING & LOCAL-TIE DETERMINATION

5.1 The Metsähovi Model

At the Onsala Space Observatory, several local-tie surveys were carried out in the 90's. However, those surveys did not provide a complete covariance matrix. In 2002 and 2008 local-tie survey were more accurate and contains complete covariance matrix of the coordinates. The main drawback of these campaigns was that they were time consuming, needed field observations and also requires a large number of equipment (i.e. laser tracker, reflector, survey pillars etc). Therefore, in 2011 an indirect approach based on GNSS developed by Finnish researchers called *The Metsähovi Model* was adopted

The basic assumptions of the model are that points in antenna structure rotate about the elevation axis and the elevation axis rotates about the azimuth axis *(Kallio & Poutanen, 2010).*

The position vector of the GNSS antenna *X* on the radio telescope in an arbitrary reference frame is the sum of three vectors: the position vector of the reference point X_0, the axis offset vector *E* rotated by angle α about the azimuth axis *a*, and a vector from the eccentric point E to the antenna point *P* rotated about the elevation axis *e* by angle ε and about the azimuth axis by the angle α, *see Figure 5.1 (Kallio & Poutanen, 2010).*Thus the basic equation becomes:

$$X - (X_0 + R_{\alpha,a}E + R_{\alpha,a}R_{\varepsilon,e}P) = 0 \qquad 5.1$$

Where X_0, E, a, e and P are the unknowns that we want to determine. The rotation matrix is described by $R_{\alpha,a}$ about the azimuth axis and $R_{\varepsilon,e}$ is the rotation matrix about the elevation axis. The GPS observations are denoted by *X (Kallio & Poutanen, 2010)*. The radio telescope azimuth and elevation angles are described by α and ε respectively. Each of the unknowns and GNSS measurements have x, y and z components of course.

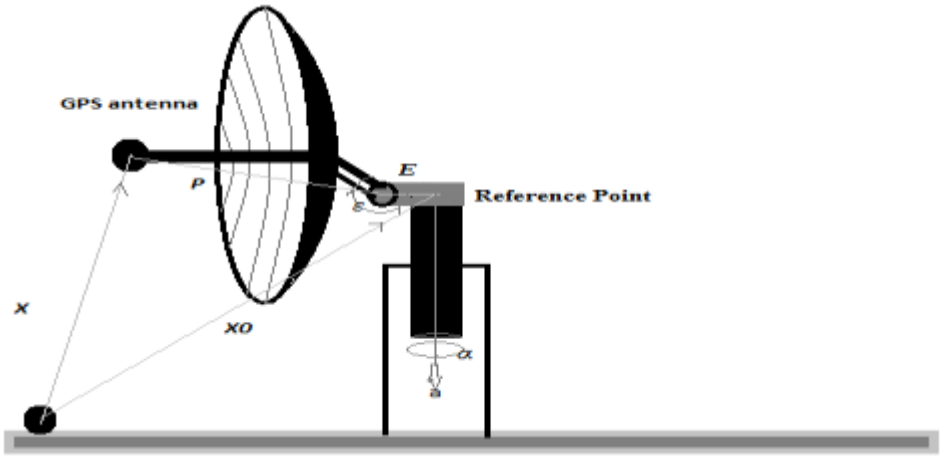

Figure 5.1: Model parameters and the local reference frame

The Rodrigues rotation formula uses the telescope angles to give the rotation *(Kallio & Poutanen, 2010)*. The rotation matrices are then:

$$R_{\alpha,a}=cos(\alpha)\begin{bmatrix}1&0&0\\0&1&0\\0&0&1\end{bmatrix}+(1-cos(\alpha))\begin{bmatrix}ax\cdot ax & ax\cdot ay & ax\cdot az\\ ax\cdot ay & ay\cdot ay & ay\cdot az\\ ax\cdot az & ay\cdot az & az\cdot az\end{bmatrix}+sin(\alpha)\begin{bmatrix}0 & -az & ay\\ az & 0 & -ax\\ -ay & ax & 0\end{bmatrix} \quad 5.2$$

$$R_{\varepsilon,e}=cos(\varepsilon)\begin{bmatrix}1&0&0\\0&1&0\\0&0&1\end{bmatrix}+(1-cos(\varepsilon))\begin{bmatrix}ex\cdot ex & ex\cdot ey & ex\cdot ez\\ ex\cdot ey & ey\cdot ey & ey\cdot ez\\ ex\cdot ez & ey\cdot ez & ez\cdot ez\end{bmatrix}+sin(\varepsilon)\begin{bmatrix}0 & -ez & ey\\ ez & 0 & -ex\\ -ey & ex & 0\end{bmatrix} \quad 5.3$$

Therefore, we have four components for each rotation matrix: three for the axis and one for the angle. The axis is a unit vector. Thus we have two condition equations for the axes parameters and two condition equations between the axes offset vector and azimuth and elevation axes *(Kallio & Poutanen, 2010).*

The azimuth axis is a unit vector:

$$ax\cdot ax + ay\cdot ay + az\cdot az - 1 = 0 \quad 5.4$$

The elevation axis is a unit vector:

$$ex\cdot ex + ey\cdot ey + ez\cdot ez - 1 = 0 \quad 5.5$$

The offset vector $\vec{E}$ is perpendicular to both $\vec{a}$ and $\vec{e}$:

$$Ex\cdot ax + Ey\cdot ay + Ez\cdot az = 0 \quad 5.6$$

$$Ex\cdot ex + Ey\cdot ey + Ez\cdot ez = 0 \quad 5.7$$

The vector of unknown parameters that we want to estimate:

$$\bar{\beta}=(\Delta Xx, \Delta Xy, \Delta Xz, \Delta Ex, \Delta Ey, \Delta Ez, \Delta ax, \Delta ay, \Delta az, \Delta ex, \Delta ey, \Delta ez, \Delta Px, \Delta Py, \Delta Pz) \quad 5.8$$

Therefore the final condition equations become:

$$(ax|_0 + \Delta ax)^2+(ay|_0 + \Delta ay)^2+(az|_0 + \Delta az)^2 = 1 \quad 5.9$$

$$(ex|_0 + \Delta ex)^2+(ey|_0 + \Delta ey)^2+(ez|_0 + \Delta ez)^2 = 1 \quad 5.10$$

$$(Ex|_0 + \Delta Ex)(ax|_0 + \Delta ax) + (Ey|_0 + \Delta Ey)(ay|_0 + \Delta ay) + (Ez|_0 + \Delta Ez)(az|_0 + \Delta az) = 0 \quad 5.11$$

$$(Ex|_0 + \Delta Ex)(ex|_0 + \Delta ex) + (Ey|_0 + \Delta Ey)(ey|_0 + \Delta ey) + (Ez|_0 + \Delta Ez)(ez|_0 + \Delta ez) = 0 \quad 5.12$$

Where, $ax|_0$, $ay|_0$, $az|_0$, $ex|_0$, $|_0$, $ez|_0$, $Ex|_0$, $Ey|_0$, $Ez|_0$ are the priori values of the axis a, *e* and offset vector *E*.

The solution of the unknown parameters is achieved by solving a least squares mixed model with the conditions between them *(Kallio & Poutanen, 2010).* The least squares mixed model also known as Gauss- Helmert model that includes all the condition equations and main function:

$$\binom{x}{k}_h = \begin{pmatrix} \sum_i^t [A_i^T (B_i p_i^{-1} B_i^T)^{-1} A_i] & HH^T \\ HH & 0 \end{pmatrix}^{-1} \begin{pmatrix} \sum_i^t [A_i^T (B_i p_i^{-1} B_i^T)^{-1} Y_i] \\ WW \end{pmatrix} \quad 5.13$$

Where, x_h is the correction to the approximate values of the parameters after *h* iteration and k is the vector of Lagrange multipliers. In the *Equation 5.13* Y_i is the basic Equation for all points in epoch *i* with approximate values of parameters *(Kallio & Poutanen, 2010).*

$$Y_i = \overrightarrow{X_i} - \overrightarrow{X_0}|_0 - R_{(\alpha,\vec{a})}|_0 \vec{E}|_0 - R_{(\alpha,\vec{a})}|_0 R_{(\varepsilon,\vec{e})}|_0 \vec{P}|_0 \quad 5.14$$

The *HH* and *WW* matrices are derived from the condition equations. Solving conditions equations and differentiating with respect to the correction, *see Equation 5.8* gives us *HH* and *WW*:

$$HH_{4\times 15} = \begin{pmatrix} 0 & 0 & 0 & 0 & 0 & 0 & ax|_0 & ay|_0 & az|_0 & 0 & 0 & 0 & 0 & 0 & 0 \\ 0 & 0 & 0 & 0 & 0 & 0 & 0 & 0 & 0 & ex|_0 & ey|_0 & ez|_0 & 0 & 0 & 0 \\ 0 & 0 & 0 & ax|_0 & ay|_0 & az|_0 & Ex|_0 & Ey|_0 & Ez|_0 & 0 & 0 & 0 & 0 & 0 & 0 \\ 0 & 0 & 0 & ex|_0 & ey|_0 & ez|_0 & 0 & 0 & 0 & Ex|_0 & Ey|_0 & Ez|_0 & 0 & 0 & 0 \end{pmatrix} \quad 5.15$$

$$WW_{4\times 1} = \begin{pmatrix} \frac{1}{2}(1 - (ax|_0)^2 - (ay|_0)^2 - (az|_0)^2) \\ \frac{1}{2}(1 - (ex|_0)^2 - (ey|_0)^2 - (ez|_0)^2) \\ -Ex|_0 ax|_0 - Ey|_0 ay|_0 - Ez|_0 az|_0 \\ -Ex|_0 ex|_0 - Ey|_0 ey|_0 - Ez|_0 ez|_0 \end{pmatrix} \quad 5.16$$

The partial differentiation with respect to the unknowns and observations will give A_i and B_i matrix respectively for epoch i*:*

$$A_i = \begin{pmatrix} \frac{\partial Y}{\partial X_0} & \frac{\partial Y}{\partial E} & \frac{\partial Y}{\partial a} & \frac{\partial Y}{\partial e} & \frac{\partial Y}{\partial P} \end{pmatrix} \quad 5.17$$

$$B_i = \begin{pmatrix} \frac{\partial Y}{\partial az_i} & \frac{\partial Y}{\partial el_i} & \frac{\partial Y}{\partial X_i} \end{pmatrix} \quad 5.18$$

p in the *Equation 5.13* is a weight matrix of the epoch *i* is:

$$p = \begin{pmatrix} \sigma_\alpha^2 & 0 & 0 \\ 0 & \sigma_\epsilon^2 & 0 \\ 0 & 0 & c_i \end{pmatrix}^{-1} \quad 5.19$$

Where, σ_α^2 and σ_ϵ^2 are variances of the telescope azimuth and elevation angles respectively. The covariance c_i can be derived from the standard deviations of the coordinate observations in epoch i.

The inverse of the normal equation matrix in the least squares adjustment is the covariance matrix of the unknown parameters of the model *(Kallio and Poutanen, 2010).*

5.2 Test Simulations and Evaluations

The Metsähovi Model was programmed and simulated in MATLAB. To start with the eccentricity vector $\vec{E}$ was taken out from the equations to simplify the task. Therefore, the

condition equations for the model reduced to two. As the azimuth axis and elevation axis are perpendicular to each other, a new condition equation was added to the model (e.g. *ax·ex+ay·ey+az·ez=0*). However, in the first simulation task a predetermined data set with no eccentricity was used and in the second simulation some eccentricity was added. In the final simulation to fit the practical case, data points above 50 degree elevation were considered. The condition equations for the eccentricity vector $\vec{E}$ were included and the eccentricity vector was determined. *Table 5.1* shows the correction to the initial values and number of iterations to achieve nominal result.

Test	*No. of Points*	*Ref. Point m*	**P** *Vector m*	*Initial Values m*	*Iterations*	*Resulting Reference Points, m*	*Resulting P Vector m*	*Noise*	*Eccentricity m*
SIM_01	1368	10	0	15	5	10.0010	0.0084	Yes	No
		15	11	15		14.9997	10.9974		
		20	0	15		20.0027	-0.0039		
SIM_02	1368	25	0	15	5	25.0001	1.0578	Yes	Yes
		15	14	15		14.9998	13.9870		
		20	0	15		19.3898	0.2912		
SIM_03	120	11	0	15	5	11.0075	-0.0964	Yes	-0.0836
		13	17	15		12.9958	16.7851		0.0212
		15	0	15		14.9491	-0.0933		-0.0513

Table 5.1: Test Simulation results

The results of the test simulations indicates that the program runs properly as expected. However a clear effect of eccentricity in the 'SIM_02' tests is visible. The ***Z*** component of the reference point deviated more than expected. For the third simulation test we have the results with eccentricity vectors. For SIM_03' test an elevation mask was used. The minimum elevation angle was 50 degree. *Figure 5.2* and *Figure 5.3* shows projected reference point of SIM_01 and SIM_03 test simulations respectively.

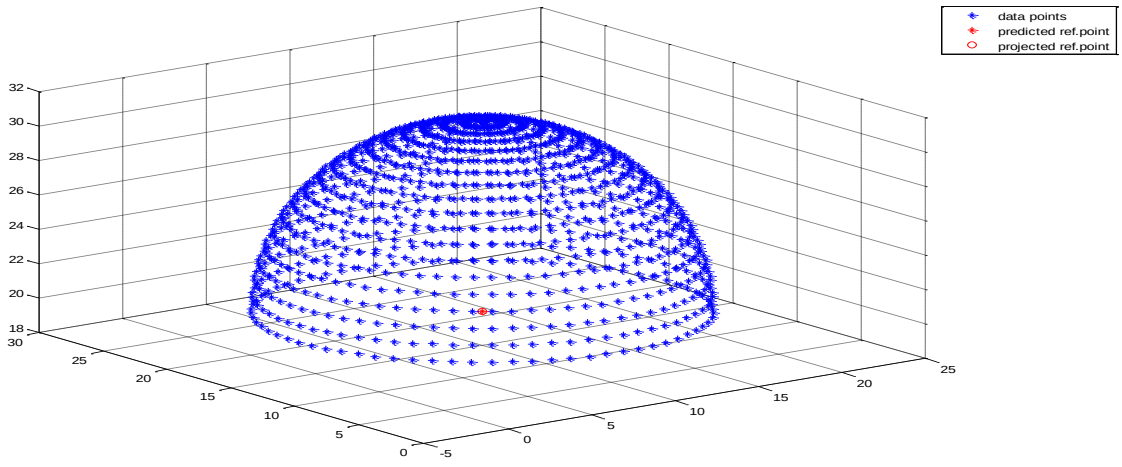

Figure 5.2 Simulated reference point for SIM_01

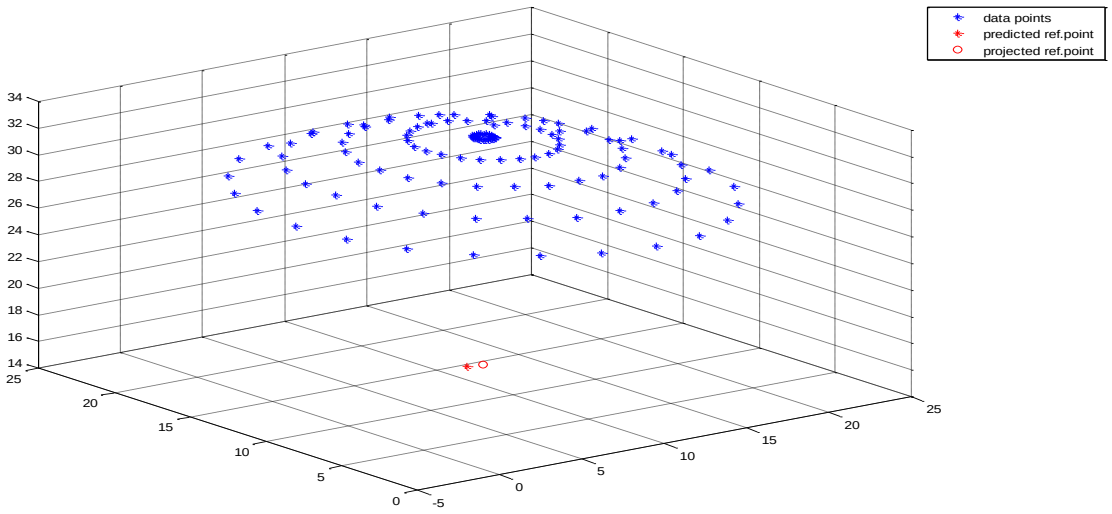

Figure 5.3: Simulated reference point for SIM_03

Comparing the three test simulations one can make a conclusion that to acquire precise result we do need enough data that forms half of a sphere. We could look at the covariance matrix of the test simulations and observe the coordinate variances. The order of elements are: top row- σ_{xx}^2, σ_{xy}^2, σ_{xz}^2 middle row- σ_{yx}^2, σ_{yy}^2, σ_{yz}^2 bottom row- σ_{zx}^2, σ_{zy}^2, σ_{zz}^2 and units are in m^2.

Cov_SIM_01= 1.0e-011 ×

$$\begin{pmatrix} 0.0007 & -0.0000 & -0.0000 \\ -0.0000 & 0.0008 & 0.0000 \\ -0.0000 & 0.0000 & 0.1547 \end{pmatrix}$$

Cov_SIM_02= 1.0e-010 ×

$$\begin{pmatrix} 0.0001 & -0.0000 & -0.0000 \\ -0.0000 & 0.0001 & -0.0000 \\ -0.0000 & -0.0000 & 0.1676 \end{pmatrix}$$

Cov_SIM_03= 1.0e-006 ×

$$\begin{pmatrix} 0.0000 & -0.0000 & 0.0001 \\ -0.0000 & 0.0000 & -0.0001 \\ 0.0001 & -0.0001 & 0.3737 \end{pmatrix}$$

We expect to have larger variance of *'z'* component of *'SIM_03'* because we have data that only cover the top of the sphere.

5.3 Preparation of Data

The performance of *The Metsähovi Model* largely depends on the observed data quality. The GIPSY OASIS v 5.0 was used in kinematic mode with 30 sec sampling for GPS data processing. One very important fact that has to be taken care of data collected when the radio telescope was moving has to be removed from the data set. The ordinary VLBI sessions require more care than that of GPS sessions because of its instability in one position. Therefore, we have considered data collected only when the radio telescope was observing target. Furthermore, data were also rejected when the radio telescope was elevated lower than 30 degree. This was done to remove more noisy data. During the GNSS sessions telescope was stable in one direction for 30 minutes, allowing us to collect more data in a particular position of the radio telescope than a VLBI session. For the final analysis data points with a standard deviation larger than 10 cm were removed. For particular azimuth and elevation angle a mean position of the radio telescope was taken. However, after data processing it was found that GNSS observations done during ordinary the VLBI sessions have very large standard deviations (i.e. ≥ tens of centimeters) whereas during the GNSS sessions solution gives reasonable standard deviation. Therefore, it was not possible to consider GNSS observations done during VLBI sessions and that restricts acquiring enough quality data for simulation in the model. The GNSS observations conducted during seven GNSS sessions in February and March 2011 were considered.

Session	*Total Data Points*	*Selected Data Points*
APEX_110223	480	6
APEX_110224	480	8
APEX_110225	960	11
APEX_110226	360	4
APEX_110322	480	7
APEX_110323	1800	22
APEX_110324	360	4

Table 5.2: Collected data and accepted data for processing

5.4 GNSS Data Analysis

The data points we have from the GIPSY solution they are refereing to the geocentric coordinate system. Whereas, *The Metsähovi Model* was modeled and programmed for the local reference frame, referring to the topocentric coordinate system. Therefore, it requires to covert the GIPSY solution into local topocentric coordinate system or make the model work for the global

geocentric coordinate system. However, an additional rotation matrix was included in the basic equation of the model in order to make it valid for geocentric coordinate system.

$$X - (X_0 + R_e\, R_{\alpha,a} E + R_{\varepsilon,e} R_{\alpha,a} R_e P) = 0 \quad (5.1)$$

Where,

$$R_e = \begin{pmatrix} -\sin(\lambda) & -\sin(\Phi)\cos(\lambda) & \cos(\Phi)\cos(\lambda) \\ \cos(\lambda) & -\sin(\Phi)\sin(\lambda) & \cos(\Phi)\sin(\lambda) \\ 0 & \cos(\Phi) & \sin(\Phi) \end{pmatrix} \quad (5.2)$$

In the *Equation 5.2* Longitude and latitude are described by λ and Φ respectively.

As we do not have enough quality data therefore in the real data analysis eccentricity vector was not used. However, we know there is small amount of axis offset present in the system (i.e.~6 mm) *(Lösler and Haas, 2009)*. The processed data were sorted out for the analysis in two different approaches. Firstly, there were only 62 data points for the analysis that includes both February and March observations, *see Table 5.1*. For the second approach the GOA script was modified. As the field station and the IGS station are close to each other, IGS station tropospheric solutions were used for field data processing and total 629 data points were selected from 1800 observations for day 82 in the year 2011. *Table 5.3* summarizes the results of real data analysis:

Test	*No. of Points*	*Approx. Ref. Points (m)*	*Approx.* **P** *Vector* (m)	*Resulting Ref. Points (m)*	*Resulting P Vector(m)*
App_01	62	3370605.9621	0	3370605.7508	-0.0124
		711917.5670	0	711917.7159	13.2870
		5349830.7985	0	5349830.7784	0.0685
App_02	629	3370605.9621	0	3370605.8201	-0.0134
		711917.5670	0	711917.7075	13.2748
		5349830.7985	0	5349830.8730	0.0590

Table 5.3: Real data analysis results

From analysis, the level of accuracy achieved was not so precise. Resulting ***P*** vector is within acceptable mark ($\sim 13.5\ m$). It should indeed be possible to achieve more accurate result with enough quality observations. *Figure 5.4* shows residuals as a function of epoch (*APP_02*);

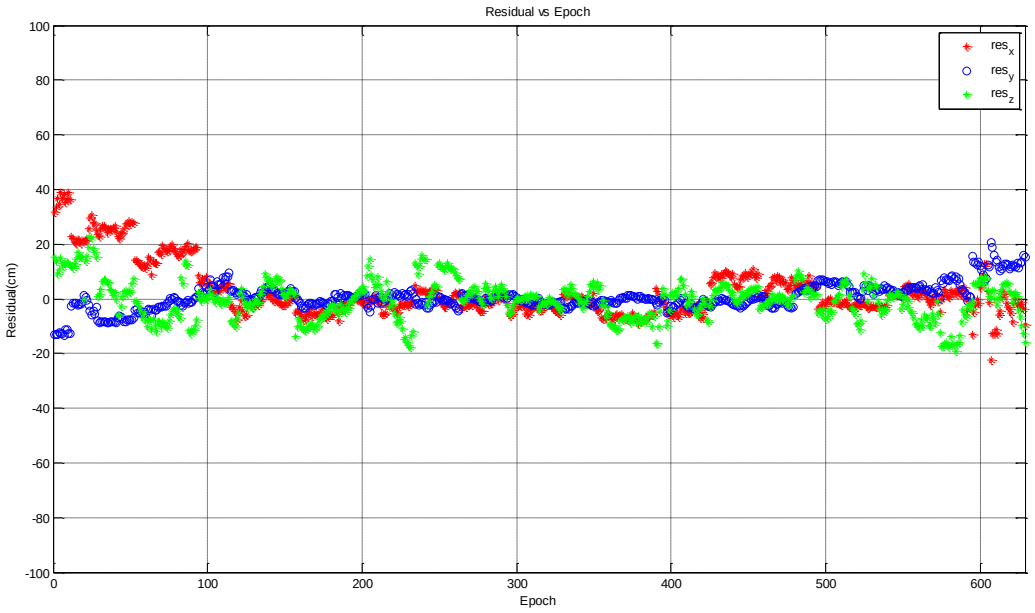

Figure 5.4: Residual plot with respect to epoch

The residuals are expected to be closer to 0. However, most of the residuals are within the range of ±40 centimeters. *Figure 5.5* shows residuals with respect to elevation, which might be an interesting thing to observe as the GNSS antenna was titled in several elevation angles therefore we would be able to notice elevations that are causing larger residual and can be treated as outliers. When the elevation of the radio telescope is in the higher side, the residuals are within ± 5 centimeters whereas the residuals of *Z* component are still large. And the scale of residual distribution for all three components gradually increases when the radio telescope elevation is in the lower side, summarizing that we can only get quality observations when the telescope is at high elevation.

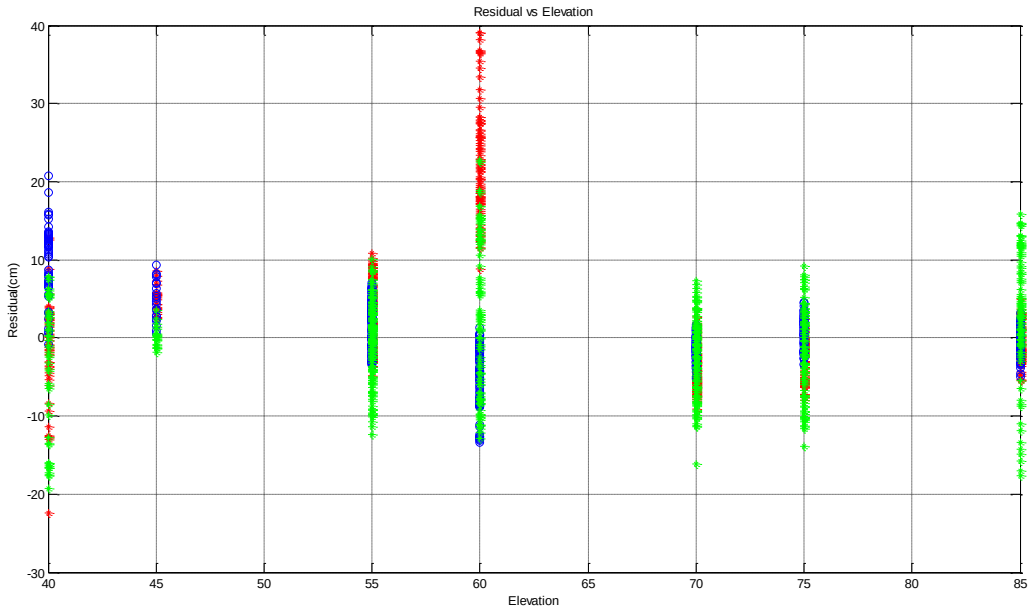

Figure 5.5: Residuals with respect to elevation

Figure 5.6 shows a relative comparison of residuals with respect to azimuth.

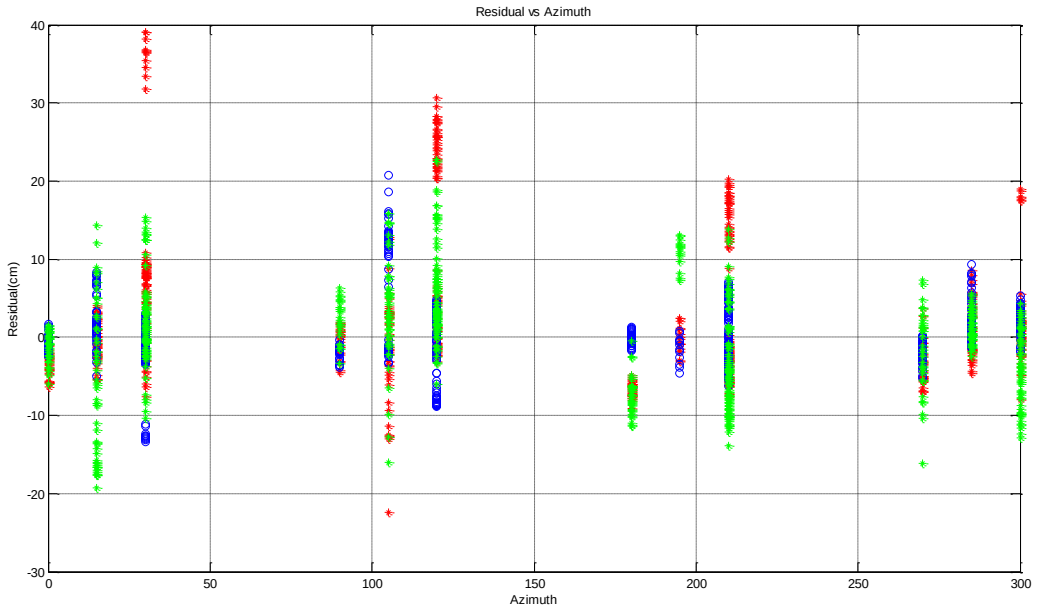

Figure 5.6: Residuals with respect to azimuth

5.5 Results and Comparison

In the previous section we discussed about the solutions achieved using the MATLAB based analyzing software. In real data analysis, it was not possible to get accurate results. However between App_01 and App_02 test data we would rather trust App_02 results. In App_02, we have more observations and elevation covered 40 to 85 degrees. However after the first iteration, larger residuals (i.e. ≥ 15 cm) were considered as the outliers and taken out from the analysis. After removing the outliers the observations were analyzed again. *Table 5.4* shows the 20 meter radio telescope reference point comparison between 2002, 2008 and 2011 measurements. The standard deviations of the coordinates are also compared.

Campaign	***X (m)***	***σ_x(mm)***	***Y(m)***	***σ_y(mm)***	***Z(m)***	***σ_z(mm)***
2002	3370605.9602	±0.1	711917.5650	±0.1	5349830.8018	±0.1
2008	3370605.9622	±01.5	711917.5671	±01.6	5349830.7986	±01.6
2011	3370605.9621	± 0.69	711917.5667	± 0.37	5349830.7984	± 0.85

Table 5.4: IVS station IVP comparison

The model also gives the complete covariance matrix between coordinate parameters of the IVS station in the geocentric Cartesian system. The order of elements are: top row- σ_{xx}^2,σ_{xy}^2, σ_{xz}^2 middle row- σ_{yx}^2, σ_{yy}^2, σ_{yz}^2 bottom row- σ_{zx}^2, σ_{zy}^2, σ_{zz}^2 and units are $10^{-6}\ m^2$.

0.4695	0.1791	0.5322
0.1791	0.1394	0.2237
0.5322	0.2237	0.7170

Table 5.5: Covariance matrix of the coordinate parameters

Corresponding correlation matrix;

1.0000	0.7001	0.9173
0.7001	1.0000	0.7076
0.9173	0.7076	1.0000

Table 5.6: Correlation matrix of the coordinate parameters

CHAPTER SIX- CONCLUSIONS AND OUTLOOK

This chapter contains the conclusion of the thesis work and recommendations for the future work. The thesis work was conducted in two parts, phase center correction of a tilted GNSS antenna and determining the reference point of the 20 meter radio telescope using the *The Metsähovi Model.*

6.1 Conclusion and Recommendations for the PCV Correction Software

As the noise inside the radome was dominating the GNSS observations rather exceedingly, the PCV corrections were not applied to the final analysis. However, PCV corrections should be applied to the analysis. It was not possible to measure the performance of the software due to corrupted data. It should be possible to do the performance test of the JAVA software of a tilted GNSS antenna where the received signal does not face unusual blockage (outside radome).

The GNSS observables in a RINEX file also differ with receiver type. The software was built following the RINEX file format that ASHTECH UZ-12 receiver provided. The format of the RINEX file from LEICA GRX1200 was different; therefore a modification of the software is needed. The software also does not account for GLONASS. It might also be possible to add GLONASS satellites in the software too. However, if it is not possible then one can remove GLONASS from the receiver and only do GPS observations and run the PCV correction software.

6.2 Conclusion and Recommendations for the Local-Tie Determination Model

To determine the reference point of the 20 meter radio telescope at OSO *The Metsähovi Model* was adopted and modeled. The model was programmed and simulated in MATLAB. Several test simulations were performed to observe the performance of the analysis software. The test simulation results indicate that the software was coded without bugs. However, the real data analysis did not provide a precise result. It was expected to be more accurate. One obvious problem was the GNSS antenna did not maintain a constant horizontal position. An alternative approach is to use Gimbaled GNSS antennas on edge of the main reflector of the radio telescope. This mount will enable the GNSS antennas to stay vertical and also allow receiving quality observations while the radio telescope elevation is low. With a tilted GNSS antenna it was impossible to accept any observation below 40^{o} elevation. *Figure 6.1* shows precision of the reference point determination improvement as a function of targets (i.e. GNSS antennas) and number of antenna positions.

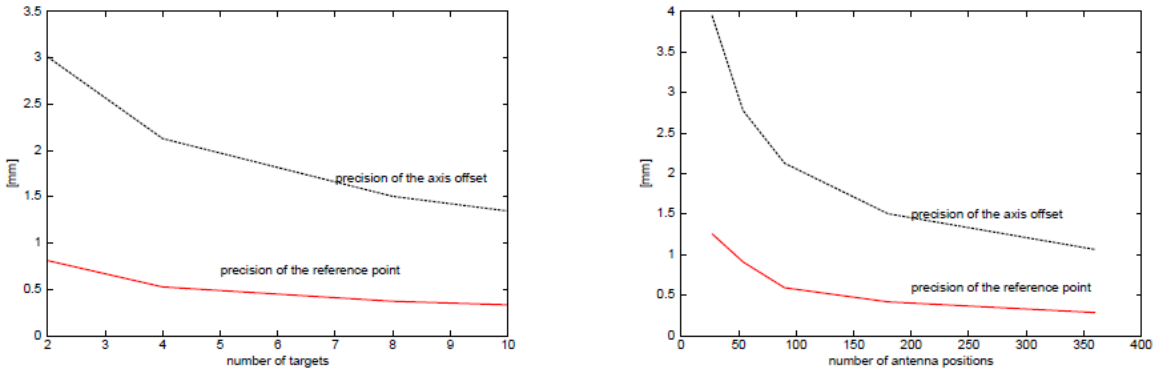

Figure 6.1: Precision of the reference point as a function of targets (left) and precision of the reference point as a function of antenna positions (right) (Kallio and Poutanen, 2010).

In the thesis work GIPSY OASIS v5.0 in kinematic mode with 30 sec sampling rate was used for GNSS data processing. Other processing software should be used to process GPS data. This will enable us to it figure out which software is best for such experiment. The Position Dilution of Precision (PDOP) should also be considered for satellite geometry. In order to carry out a static GPS observation, the radio telescope should be placed in number of predetermined positions for 1 hour session. Precise observations will lead to more accurate reference point determination.

REFERENCES

Altamimi Z., Sillard P., Boucher C. (2002) ITRF2000: *a new release of the international terrestrial reference frame for earth science application.* J Geophys Res 107(B10):2214. DOI 10.1029/2001JB000561

Bergstrand S., Haas R., Johansson J. (2000): *A New GPS- VLBI Tie at the Onsala Space Observatory,* IVS 2000 General Meeting Proceedings, p. 128-132

Chong C. (2009), Status of COMPAS/BeiDou Development, *Stanfords 2009 PNT Challenges and Opportunities Symposium,* October 21-22 2009, presentation, San Francisco, USA

Dach, R., Hugentobler U., Fridez P., and Meindl M. (Eds.) (2007): *Bernese GPS Software Version 5.0,* Astronomical Institute, University of Bern.

Dawson J., Sarti P., Johnston G., Vittuari L. (2007): *Indirect approach to invariant point determination for SLR and VLBI systems: an assessment.* J Geod 81:433-441. DOI 10.1007/s00190-006-0125-x

El-Rabbany, A. (2002): *Introduction to GPS: The Global Positioning System*. Artech House Publishers, Boston, USA. ISBN 1-58053-183-0

El-Rabbany, A. (2003): *Precise GPS Point Positioning: the Future Alternative to Differential GPS Surveying.* Ontario Professional Surveyor, Vol. 45, No. 4, pp. 11-13

ESA Galileo Navigation, (2007), Full deployment, *European Space Agency*, available from http://www.esa.int/esaNA/galileo.html

Eschelbach C. and Haas R. (2005): *The 2002 Local Tie Survey at the Onsala Space Observatory.* In: Proc. IERS Workshop on site co-location, edited by B. Richter, W. Schwegmann and W.R. Dick, IERS Technical Note, 33, Verlag des Bundesamts für Kartographie und Geodäsie, 55-63

Inside GNSS, (2010), Russia Reveals CDMA Signal Plan as GLONASS Nears Full Operational Capacity, *Inside GNSS*, November/ December issue, Gibbons Media & Research LLC, United States, available from http://www.insidegnss.com/node/2355

Kallio U. and Poutanen M. (2010):"*Can we really promise a mm-accuracy for the local ties on a geo-VLBI antenna",* submitted to IAG proceedings, 2009

Kallio U. and Poutanen M. (2010): *Simulation of local tie accuracy on VLBI antennas.* In VLBI2010: From Vision to Reality (Ed. Dirk Behrend and Karen Baver). Sixth IVS General Meeting February 7-13, 2010, Hobart, Australia. NASA/CB-2010-215864, p. 360-364

Löfgren J. S. (2011): *Observing Sea Level Using Reflected Global Navigation Satellite System Signals*, Thesis for the Degree of Licentiate of Engineering, Technical Report No. 42L, Department of Earth and Space Science, Chalmers University of Technology, Gothenburg, SE

Lösler M. and Haas R. (2009): *The 2008 Local-tie Survey at the Onsala Space Observatory*. In Charlot P., A. Collioud and G. Bourda, G. (Ed.) Proceedings of the 19th European VLBI for Geodesy and Astrometry Working Meeting, March 24–25, 2009, Bordeaux, France, p. 97–101

Lösler M. and Eschelbach C. (2009): *Evaluation and obtained expertise in reference point determination at the GIK*. In Charlot P., A. Collioud and G. Bourda, G. (Ed.) Proceedings of the 19th European VLBI for Geodesy and Astrometry Working Meeting, March 24–25, 2009, Bordeaux, France, p. 116–121

Niell A., Whitney A., Petrachenko B., Schlüter W., Vandenberg N., Hase H., Koyama Y., Ma C., Schuh H. and Tuccari G. (2006) VLBI2010: *Current and Future Requirements for Geodetic VLBI Systems.* In: IVS Annual Report 2005, edited by D. Behrend and K. Baver, NASA/TP-2006-214136, 13-40

Ray J., Altamimi Z. (2005): *Evaluation of co-location ties relating the VLBI and GPS reference frames.* J Geod 79: 189-195. DOI 10.1007/s00190-005-0456-z

Rizos C. (1999): *Introduction to GPS*, University of New South Wales, Sydney. http://www.gmat.unsw.edu.au/snap/gps/gps_notes1.pdf

The GPS System (2009): *Sources of Errors in GPS*, available from, http://www.kowoma.de/en/gps/errors.htm

Teunissen P. J. G. and Kleusberg (1998), *GPS for Geodesy, 2nd Edition*, Springer, Berlin, 66 pp.

Webb F. H., Zumberge, J. F. (1993): *An Introduction to GIPSY/OASIS-II Precision Software for the Analysis of Data from the Global Positioning System*, JPL Publ. No D-11088

Zumberge J. F., Heftin M. B., and Jefferson D.C., Watkins M. M. (1997): *Precise point positioning for the efficient and robust analysis of GPS data from large networks*, Journal of Geophysical Research (102), NO. B3, 5005-5017

APPENDIX

MATLAB Codes for the Metsähovi Model

1.

```
function [Ra]=rot_a(alpha,ax,ay,az)

%Rodrigues rotation matrix
%calculates the rotation matrix of the azimuth axis
%alpha=azimuth
%ax=x coordinate of azimuth axis
%ay=y coordinate of azimuth axis
%az=z coordinate of azimuth axis

Ra = cosd(alpha)*[1 0 0
                  0 1 0
                  0 0 1
                  ]+(1-cosd(alpha))*[ax*ax ax*ay ax*az
                                     ax*ay ay*ay ay*az
                                     ax*az ay*az az*az]+sind(alpha)*[0 -az ay
                                                                     az 0 -ax
                                                                    -ay ax 0];
end
```

2.

```
function [Rb]=rot_b(theta,ex,ey,ez)

%Rodrigues rotation matrix
%calculates the rotaion matrix of the elevation axis
%theta=elevation
%ex=x coordinate of elevation axis
%ey=y coordinate of elevation axis
%ez=z coordinate of elevation axis

Rb = cosd(theta)*[1 0 0
                  0 1 0
                  0 0 1
                  ]+(1-cosd(theta))*[ex*ex ex*ey ex*ez
                                     ex*ey ey*ey ey*ez
                                     ex*ez ey*ez ez*ez
                                     ]+sind(theta)*[0 -ez ey
                                                    ez 0 -ex
                                                   -ey ex 0
                                                    ];
End
```

3.

```
function [Re]=rot_e(lat,lon)
%lat=latitude of the observations
%lon=longitude of the observations
%rot_e, is a rotational matix that converts topocentric coordinate system to  to
%geocentric coordinate system

Re=[-sin(lon) -sin(lat)*cos(lon) cos(lat)*cos(lon);cos(lon) -sin(lat)*sin(lon)
cos(lat)*sin(lon);0 cos(lat) sin(lat)];
end
```

4.

```
function [D_ax]=diffAx(alpha,theta,ax,ay,az,ex,ey,ez,lat,lon,Ex,Ey,Ez,Px,Py,Pz)

% Determines the partial differentiation of the main function with respect to 'ax'
% Rb = Rotaion matrix of the elevation axis
% Re = Rotation matrix that converts topocentric coordinate system to
% geocentric coordinate system

Rb = cosd(theta)*[1 0 0
                  0 1 0
                  0 0 1]
+(1-cosd(theta)) *[ex*ex ex*ey ex*ez
  ex*ey ey*ey ey*ez
  ex*ez ey*ez ez*ez]+ sind(theta)*[0 -ez ey;ez 0 -ex; -ey ex 0];


Re=[-sin(lon) -sin(lat)*cos(lon) cos(lat)*cos(lon);cos(lon) -sin(lat)*sin(lon)
cos(lat)*sin(lon);0 cos(lat) sin(lat)];



X=Re*((1-cosd(alpha)).*([2*ax ay az
                         ay  0  0
                         az  0  0])+(sind(alpha).*[0 0 0
                                                   0 0 -1
                                                   0 1 0]))*[Ex;Ey;Ez];

C=Re*((1-cosd(alpha)).*([2*ax ay az
                         ay  0  0
                         az  0  0])+(sind(alpha).*[0 0 0
                                                   0 0 -1
                                                   0 1 0]))*Rb;

  Y=C*[Px
       Py
       Pz
       ];

   D_ax=-X-Y;
end
```

5.

```
function [D_ay]=diffAy(alpha,theta,ax,ay,az,ex,ey,ez,lat,lon,Ex,Ey,Ez,Px,Py,Pz)

% Determines the partial differentiation of the main function with respect to 'ay'
% Rb = Rotaion matrix of the elevation axis
% Re = Rotation matrix that converts topocentric coordinate system to
% geocentric coordinate system

Re=[-sin(lon) -sin(lat)*cos(lon) cos(lat)*cos(lon);cos(lon) -sin(lat)*sin(lon)
cos(lat)*sin(lon);0 cos(lat) sin(lat)];

Rb = cosd(theta)*[1 0 0
                  0 1 0
                  0 0 1]+(1-cosd(theta))*[ex*ex ex*ey ex*ez
                                          ex*ey ey*ey ey*ez
                                          ex*ez ey*ez ez*ez]+sind(theta)*[0 -ez ey
                                                                          ez 0 -ex
                                                                          -ey ex 0];

X=Re*((1-cosd(alpha)).*([0 ax 0
                         ax  2*ay  az
                         0  az  0])+(sind(alpha).*[0 0 1
                                                   0 0 0
                                                  -1 0 0]))*[Ex;Ey;Ez];
```

```
C=Re*((1-cosd(alpha)).*([0 ax 0
                        ax  2*ay  az
                        0  az  0])+(sind(alpha).*[0 0 1
                                                  0 0 0
                                                 -1 0 0]))*Rb;

Y=C*[Px
     Py
     Pz];


   D_ay=-X-Y;
end
```

6.

```
function[D_az]=diffAz(alpha,theta,ax,ay,az,ex,ey,ez,lat,lon,Ex,Ey,Ez,Px,Py,Pz)

% Determines the partial differentiation of the main function with respect to 'az'
% Rb = Rotaion matrix of the elevation axis
% Re = Rotation matrix that converts topocentric coordinate system to
% geocentric coordinate system

Re=[-sin(lon) -sin(lat)*cos(lon) cos(lat)*cos(lon);cos(lon) -sin(lat)*sin(lon)
cos(lat)*sin(lon);0 cos(lat) sin(lat)];

Rb = cosd(theta)*[1 0 0
                  0 1 0
                  0 0 1]+(1-cosd(theta))*[ex*ex ex*ey ex*ez
                                          ex*ey ey*ey ey*ez
                                          ex*ez ey*ez ez*ez]+sind(theta)*[0 -ez ey
                                                                          ez 0 -ex
                                                                          -ey ex 0];


X=Re*((1-cosd(alpha)).*([0 0 ax
                        0 0 ay
                        ax ay 2*az])+(sind(alpha).*[0 -1 0
                                                    1 0 0
                                                    0 0 0]))*[Ex;Ey;Ez];



C=Re*((1-cosd(alpha)).*([0 0 ax
                        0 0 ay
                        ax ay 2*az])+(sind(alpha).*[0 -1 0
                                                    1 0 0
                                                    0 0 0]))*Rb;

  Y=C*[Px
       Py
       Pz
       ];

   D_az=-X-Y;
end
```

7.

```
function[D_ex]=diffEx(alpha,theta,ax,ay,az,ex,ey,ez,lat,lon,Px,Py,Pz)

% Determines the partial differentiation of the main function with respect to 'ex'
% Ra = Rotaion matrix of the azimuth axis
```

```
% Re = Rotation matrix that converts topocentric coordinate system to
% geocentric coordinate system

Re=[-sin(lon) -sin(lat)*cos(lon) cos(lat)*cos(lon);cos(lon) -sin(lat)*sin(lon)
cos(lat)*sin(lon);0 cos(lat) sin(lat)];

Ra = cosd(alpha)*[1 0 0
                  0 1 0
                  0 0 1
                  ]+(1-cosd(alpha))*[ax*ax ax*ay ax*az
                                     ax*ay ay*ay ay*az
                                     ax*az ay*az az*az
                                     ]+sind(alpha)*[0 -az ay
                                                    az 0 -ax
                                                   -ay ax 0
                                                    ];

A=(1-cosd(theta).*[2*ex ey ez
                      ey  0  0
                      ez  0  0])*[Px
                                  Py
                                  Pz];
B=(sind(theta).*[0 0 0
                 0 0 -1
                 0 1 0])*[Px
                          Py
                          Pz];

D_ex=-Re*Ra*(A+B);
end
```

8.

```
function[D_ey]=diffEy(alpha,theta,ax,ay,az,ex,ey,ez,lat,lon,Px,Py,Pz)

% Determines the partial differentiation of the main function with respect to 'ey'
% Ra = Rotaion matrix of the azimuth axis
% Re = Rotation matrix that converts topocentric coordinate system to
% geocentric coordinate system

Re=[-sin(lon) -sin(lat)*cos(lon) cos(lat)*cos(lon);cos(lon) -sin(lat)*sin(lon)
cos(lat)*sin(lon);0 cos(lat) sin(lat)];

Ra = cosd(alpha)*[1 0 0
                  0 1 0
                  0 0 1
                  ]+(1-cosd(alpha))*[ax*ax ax*ay ax*az
                                     ax*ay ay*ay ay*az
                                     ax*az ay*az az*az
                                     ]+sind(alpha)*[0 -az ay
                                                    az 0 -ax
                                                   -ay ax 0
                                                    ];

A=(1-cosd(theta).*[0 ex 0
                   ex 2*ey ez
                   0 ez 0])*[Px
                             Py
                             Pz];
B=(sind(theta).*[0 0 1
                 0 0 0
                -1 0 0
                ])*[Px
                    Py
                    Pz];

D_ey=-Re*Ra*(A+B);
end
```

9.

```
function[D_ez]=diffEz(alpha,theta,ax,ay,az,ex,ey,ez,lat,lon,Px,Py,Pz)

% Determines the partial differentiation of the main function with respect to 'ez'
% Ra = Rotaion matrix of the azimuth axis
% Re = Rotation matrix that converts topocentric coordinate system to
% geocentric coordinate system

Re=[-sin(lon) -sin(lat)*cos(lon) cos(lat)*cos(lon);cos(lon) -sin(lat)*sin(lon)
cos(lat)*sin(lon);0 cos(lat) sin(lat)];

Ra = cosd(alpha)*[1 0 0
                  0 1 0
                  0 0 1
                  ]+(1-cosd(alpha))*[ax*ax ax*ay ax*az
                                     ax*ay ay*ay ay*az
                                     ax*az ay*az az*az
                                     ]+sind(alpha)*[0 -az ay
                                                    az 0 -ax
                                                   -ay ax 0
                                                    ];

A=(1-cosd(theta).*[0 0 ex
                   0 0 ey
                  ex ey 2*ez])*[Px
                                Py
                                Pz];
B=(sind(theta).*[0 -1 0
                 1  0 0
                 0  0 0])*[Px
                           Py
                           Pz];

D_ez=-Re*Ra *(A+B);
end
```

10.

```
function[D_alpha]=diffAlpha(alpha,theta,ax,ay,az,ex,ey,ez,lat,lon,Ex,Ey,Ez,Px,Py,Pz)

%calculates the partial differenciation of the main function with respect
%to azimuth angle
%Rb= rotation matrix of the elevation axis
%Re= rotation matrix that converts topocentric coordinate system to
%geocentric coordinate system

Re=[-sin(lon) -sin(lat)*cos(lon) cos(lat)*cos(lon);cos(lon) -sin(lat)*sin(lon)
cos(lat)*sin(lon);0 cos(lat) sin(lat)];

Rb = cosd(theta)*[1 0 0
                  0 1 0
                  0 0 1
                  ]+(1-cosd(theta))*[ex*ex ex*ey ex*ez
                                     ex*ey ey*ey ey*ez
                                     ex*ez ey*ez ez*ez
                                     ]+sind(theta)*[0 -ez ey
                                                    ez 0 -ex
                                                   -ey ex 0
                                                    ];


X= -Re*((-sind(alpha).*[1 0 0
                        0 1 0
                        0 0 1])+(sind(alpha).*[ax*ax ax*ay ax*az
                                               ax*ay ay*ay ay*az
                                               ax*az ay*az az*az])+
```

```
(cosd(alpha).*[0 -az ay
               az 0 -ax
              -ay ax 0]))*[Ex;Ey;Ez];



Y=-Re*((-sind(alpha).*[1 0 0
                       0 1 0
                       0 0 1])+(sind(alpha).*[ax*ax ax*ay ax*az
                                              ax*ay ay*ay ay*az
                                              ax*az ay*az az*az])+(cosd(alpha).*[0 -az ay
                                                                                 az 0 -ax
                                                                                -ay ax 0]))*Rb;
  Z=Y*[Px;Py;Pz];

  D_alpha=X+Z;
end
```

11.

```
function[D_theta]=diffTheta(alpha,theta,ax,ay,az,ex,ey,ez,lat,lon,Px,Py,Pz)

%calculates the partial differenciation of the main function with respect
%to elevation angle
%Ra= rotation matrix of the azimuth axis
%Re= rotation matrix that converts topocentric coordinate system to
%geocentric coordinate system

Re=[-sin(lon) -sin(lat)*cos(lon) cos(lat)*cos(lon);cos(lon) -sin(lat)*sin(lon)
cos(lat)*sin(lon);0 cos(lat) sin(lat)];

Ra = cosd(alpha)*[1 0 0
                  0 1 0
                  0 0 1
                  ]+(1-cosd(alpha))*[ax*ax ax*ay ax*az
                                     ax*ay ay*ay ay*az
                                     ax*az ay*az az*az
                                     ]+sind(alpha)*[0 -az ay
                                                    az 0 -ax
                                                   -ay ax 0];



X=((-sind(theta).*[1 0 0
                   0 1 0
                   0 0 1
                  ])+(sind(theta).*[ex*ex ex*ey ex*ez
                                    ex*ey ey*ey ey*ez
                                    ex*ez ey*ez ez*ez
                                     ])+(cosd(theta).*[0 -ez ey
                                                       ez 0 -ex
                                                      -ey ex 0]))*[Px;Py;Pz];

D_theta=-Re*Ra*X;
end
```

12.

```
clear all;close all;clc

tic
%%The Metsähovi model to determine reference point of the radio telescope

apex_xyz=load('observationfile.txt'); %[epoch azimuth elevation X Y Z stdX stdY stdZ]
```

```
t=629;

format long

XYZ=[(1000*apex_xyz(:,4)) (1000*apex_xyz(:,5)) (1000*apex_xyz(:,6))];

LLH_APEX=[];

for m=1:t
LLH_APEXnew=xyz2lbh(XYZ(m,:));
LLH_APEX=[LLH_APEX;LLH_APEXnew];
end

% telescope apriori reference point

tel_ref(1,1)=3370605.9621;
tel_ref(1,2)=711917.5670;
tel_ref(1,3)=5349830.7985;

%set priori values of the unknowns

ax=0;
ay=0;
az=-1;

ex=1;
ey=0;
ez=0;

Px=0;
Py=0;
Pz=0;

Ex=0;
Ey=0;
Ez=0;




for k=1:1
    H=zeros(12,12);
    V=zeros(12,1);

res_x=[];
res_y=[];
res_z=[];

for l=1:t
        a=apex_xyz(l,2)+180; % telescope azimuth. add 180 deg if the az-el file is .snp file
        b=apex_xyz(l,3);     % telescope elevation

        tel_ref=[tel_ref(1,1) tel_ref(1,2) tel_ref(1,3)];

        LLH_ref=xyz2lbh(tel_ref); % covert cartesian coordinates into latitude, longitude and
hight

        lat=LLH_ref(1,2);
        lon=LLH_ref(1,1);

    %rotation matrics
    Ra=rot_a(a,ax,ay,az);
    Rb=rot_b(b,ex,ey,ez);
    Re=rot_e(lat,lon);

    %partial differenciations
    D_ax=diffAx(a,b,ax,ay,az,ex,ey,ez,lat,lon,Ex,Ey,Ex,Px,Py,Pz);
    D_ay=diffAy(a,b,ax,ay,az,ex,ey,ez,lat,lon,Ex,Ey,Ez,Px,Py,Pz);
    D_az=diffAz(a,b,ax,ay,az,ex,ey,ez,lat,lon,Ex,Ey,Ez,Px,Py,Pz);
    D_ex=diffEx(a,b,ax,ay,az,ex,ey,ez,lat,lon,Px,Py,Pz);
    D_ey=diffEy(a,b,ax,ay,az,ex,ey,ez,lat,lon,Px,Py,Pz);
```

```
    D_ez=diffEz(a,b,ax,ay,az,ex,ey,ez,lat,lon,Px,Py,Pz);
    D_alpha=diffAlpha(a,b,ax,ay,az,ex,ey,ez,lat,lon,Ex,Ey,Ez,Px,Py,Pz);
    D_theta=diffTheta(a,b,ax,ay,az,ex,ey,ez,lat,lon,Px,Py,Pz);



    %3*15 jacobian matrix of unknows
    %[DX0x DX0y DX0z DEx DEy DEz Dax Day Daz Dex Dey Dez Px Py Pz]

    A=[[-1 0 0;0 -1 0;0 0 -1] [D_ax D_ay D_az] [D_ex D_ey D_ez] -Re*Ra*Rb];


    % 3*5 jacobian matrix of observations
    % [Dalpha Dtheta DXx DXy DXz]

    B=[D_alpha D_theta [1 0 0;0 1 0;0 0 1]];


    %Variances of Azimuth and Elevation observations

       Salpha=pi/180/3600*10;
       Stheta=pi/180/3600*10;


%  standard deviations of coordinate observations in epoch i



     Gx=apex_xyz(l,7);
     Gy=apex_xyz(l,8);
     Gz=apex_xyz(l,9);

     % weight matrix

    p=pinv([Salpha.^2 0 0 0 0
            0 Stheta.^2 0 0 0
            0 0 Gx.^2 0 0
            0 0 0 Gy.^2 0
            0 0 0 0 Gz.^2]);


Hnew=(A'*pinv(B*pinv(p)*B')*A);

H=H+Hnew;

% basic equation

Y=[XYZ(l,1);XYZ(l,2);XYZ(l,3)] -[tel_ref(1,1);tel_ref(1,2);tel_ref(1,3)]-Re*Ra*[Ex;Ey;Ez]-
Re*Ra*Rb*[Px;Py;Pz];

Vnew=(A'*pinv(B*pinv(p)*B')*Y);

V=V+Vnew;




%condition equations


 HH=[0 0 0 ax ay az 0 0 0  0 0 0
     0 0 0 0 0 0   ex ey ez  0 0 0
     0 0 0 ex ey ez ax ay az 0 0 0];

  WW=[1/2*(1-ax.^2-ay.^2-az.^2)
     1/2*(1-ex.^2-ey.^2-ez.^2)
     -ax*ex-ay*ey-az*ez];
```

```
 D=[0 0 0;0 0 0;0 0 0];

 %Least square mixed model

 MM=[H HH';HH D];
 NN=[V;WW];

 X=pinv(MM)*NN;



end

% update priori values

tel_ref(1,1)=tel_ref(1,1)-X(1); tel_ref(1,2)=tel_ref(1,2)-X(2); tel_ref(1,3)=tel_ref(1,3)-X(3);
ax=ax-X(4); ay=ay-X(5); az=az-X(6);ex=ex-X(7);ey=ey-X(8);ez=ez-X(9);
Px=Px-X(10); Py=Py-X(11); Pz=Pz-X(12);



XXi=[tel_ref(1,1);tel_ref(1,2);tel_ref(1,3)]+Re*Ra*Rb*[Px;Py;Pz];

% look for residuals


for d=1:t
          aa=apex_xyz(d,2)+180;
        bb=apex_xyz(d,3);

    Raa=rot_a(aa,ax,ay,az);
    Rbb=rot_b(bb,ex,ey,ez);
    tel_ref_new=[tel_ref(1,1) tel_ref(1,2) tel_ref(1,3)];
    LLH_ref_new=xyz2lbh(tel_ref_new);

        lat=LLH_ref_new(1,2);
        lon=LLH_ref_new(1,1);
      Ree=rot_e(lat,lon);
    XXi=([tel_ref_new(1,1);tel_ref_new(1,2);tel_ref_new(1,3)]+Ree*Raa*Rbb*[Px;Py;Pz])';
    res=XXi-[XYZ(d,1) XYZ(d,2) XYZ(d,3)];

    res_xnew=res(1,1);
    res_ynew=res(1,2);
    res_znew=res(1,3);
    res_x=[res_x;res_xnew];
    res_y=[res_y;res_ynew];
    res_z=[res_z;res_znew];
    RES=[res_x res_y res_z];
end
end
% plot residuals


figure
plot(res_x*100,'r*');
hold on
plot(res_y*100,'bo');
hold on
plot(res_z*100,'g*');
grid on
xlabel('Epoch')
ylabel('Residual(cm)')
axis([0 629 -100 100]);
title('Residual vs Epoch')

toc

%%%%%%%%%%%%%%%%%%%%%%%%%%%%%%%%%%%%%%%%%%%%%%%%%%%%%%%%%%%%%%%%%%%%%%%%%%%%%%%
```